Black carbon aerosols at an urban site in North Africa (Kenitra, Morocco)

Youssef Bounakhla[2], Abdelfettah Benchrif[1,*], Mounia Tahri[1], Francesca Costabile[3], Fatiha Zahry[1], Moussa Bounakhla[1], El Kafssaoui El Hassan[2],

[1] National Centre for Nuclear Energy, Science and Technology (CNESTEN), Morocco

[2] Faculty of Sciences, Ibn Tofail University, Kenitra, Morocco

[3] Institute for Atmospheric Sciences and Climate (ISAC), National Research Council (CNR), Rome, Italy

Abstract:

Although black carbon is one of the most important atmospheric particulate components driving climate change and air quality, there is a lack of comprehensive air quality data from North African urban areas. Seven-wavelength aethalometer-collected data were used to provide first insights into the levels and patterns of equivalent black carbon (eBC) mass concentrations, particularly into the seasonal and diurnal cycles, that exist over an urban area in the North of Africa, Kenitra city, Morocco. The average BC mass concentration was observed as 0.90 ± 0.80 µg/m^3. This BC value is overall largely lower than reported African and European urban location levels, although the role of COVID-19 restrictions could have influenced this result. The diurnal pattern revealed two BC peaks corresponding to morning and evening traffic rush hours. This variation is found to be seasonally dependent, with the maximum daily amplitude occurring in winter. The BC bimodal behaviour is observed in all the seasons but with varying degrees of the magnitude of the peaks (winter>autumn>summer). This observed seasonal heterogeneity was explained by varying meteorological conditions (wind speed, wind direction, relative humidity, air pressure, air temperature, rainfall, and boundary layer height), and air mass trajectory height and pathways. It was pointed out that the daily and seasonal variations are significantly influenced by local traffic sources, wind speed, and boundary layer dynamics. Hysplit backward trajectories revealed that the long-range aerosols transport through both south-western (Atlantic region), and western (over populated areas) regions can as well contribute to BC concentrations, although to a different extent. Finally, a common thread that runs through seasonal, and diurnal variations were that typical low hourly BC concentrations (distinguished in the afternoon) do not exceed the value of 0.5 µg/m^3 representing a kind of urban background level.

Keywords: Carbonaceous aerosol; Black carbon; Aethalometer; Temporal variation; Morocco.

Highlights:

- Real-time measurements of black carbon at a North African urban site, Kenitra city.
- Low BC levels were observed in Kenitra compared with other African areas.
- A well-defined diurnal and significant seasonal variation in BC concentration.
- Local traffic activities assumed the major source of BC at the sampling site.
- Long-range sources were found to be more prominent during winter.

Corresponding author: benchrif@cnesten.org.ma

1. Introduction:

Carbonaceous aerosol is a major, sometimes dominant, constituent of atmospheric particulate matter (PM) in urban areas (Querol et al., 2013; Reche et al., 2012; Genga et al., 2017). It is primarily produced by three processes: wood combustion, fossil fuel combustion, and biogenic emissions. Carbonaceous aerosols are commonly divided into organic carbon (OC), and a refractory light-absorbing fraction known as elemental carbon (EC, when assessed using thermal-optical methods) or black carbon (BC, when quantified using optical methods). Black carbon in itself has received a lot of attention in recent decades because of its remarkable impact on regional-to-global climate change (Martinsson et al., 2017; Gatari et al., 2019; Pani et al., 2020). It is characterized as a by-product of incomplete combustion of fossil fuels in transportation engines, thermal power plants, and biomass in the residential sector, as well as smoke from agricultural and forest fires. Janssen et al. (2011) stated that combining BC measurements with other air quality indicators is advantageous since BC concentrations, as a specific indicator of local combustion sources, can reveal more about the health effects of aerosols than PM, which does not just come from burning. WHO global air quality guidelines stated that even though black carbon may not be the causal agent, it is considered as a useful additional air quality metric for assessing the health risks of primary combustion aerosols from traffic, which are not fully taken into account by $PM_{2.5}$ mass levels (WHO global air quality guidelines, 2021). In addition, there is more evidence of health effects linked to combustion sources than non-combustion sources (Segersson et al., 2017). In a recent report, the World Health Organization (WHO) reported pieces of evidence linking black carbon particles to cardiovascular health effects and premature mortality, for both short-term (24-hour) and long-term (yearly) exposures (WHO global air quality guidelines, 2021). Although insufficient data are available to provide recommendations for air quality guideline levels and interim targets, WHO warranted more actions to enhance further research on BC risks and approaches for mitigation, and outlined good practice statements for addressing BC in air quality monitoring networks (WHO global air quality guidelines, 2021).

BC temporal characteristics have long been a popular topic among researchers. Several investigations have looked at the peculiarities of BC mass concentration in different parts of Africa (Table 1), such as Tetouan (Morocco), Bou Ismaïl (Algeria), Mbour and Dakar (Senegal), Bamako (Mali), Cotonou (Benin), Yaounde (Cameroon), Nairobi and Nanyuki (Kenya), Kwadela (South Africa), Abidjan (Ivory Coast). For instance, in northern Morocco, Benchrif et al. (2018) reported that the carbonaceous particles account for 18% to 22% of the fine aerosol mass and range between 3.01 - 3.22 $\mu g/m^3$, regarding the aerosol transport pathways and their loading region. In Kenya, Gatari et al. (2003) reported that the measured concentration of BC in urban Nairobi (2.37 ± 0.3 $\mu g/m^3$) was almost twice that of rural Meru (1.47 ± 0.1 $\mu g/m^3$). They claimed that local biomass burning was the primary source of BC at all measurement sites, although emissions from vehicles and waste burning in Nairobi may have enhanced the carbonaceous aerosols. Djossou et al. (2018) revealed mean BC concentration in Abidjan ranged from about 2 ± 1 $\mu g/m^3$ near two-wheeled vehicles areas to approximately 7 ± 4 $\mu g/m^3$ in four-wheeled vehicles site. Additionally, the characterization of BC mass concentration in a low-income settlement from Kwadela in South Africa by Xulu et al. (2020) was found to show seasonal variation, where the BC level was 2.9 times higher in winter (1.89 ± 0.5 $\mu g/m^3$) than in summer (0.66 ± 0.2 $\mu g/m^3$). However, those datasets were the first attempts to assess BC in Africa, and more long-term datasets with time resolution consistent with BC lifetime in the atmosphere are needed.

To date, multiple studies have shown that two key elements, namely source emissions and meteorological conditions, can influence the concentration levels and variations of BC, the role of long-transport air masses being also relevant. For instance, in urban environments, fossil fuel combustion mainly from the vehicle and industrial emissions is the major source of BC, while in rural areas it could be linked to biomass and biofuel combustion (Zotter et al., 2017). However, in many urban and suburban areas, biomass combustion, from forest fires (in summer) or domestic heating (in winter) may also contribute significantly to BC levels (Kalogridis et al., 2018). In Africa, the dominant sources of carbonaceous aerosols in urban settings are overall fossil fuel combustion and biomass burning. In urban Kenya, Gatari et al. (2003) have identified the local biomass burning, while in the coastal towns of southern West Africa, fossil fuels come from traffic, waste burning at landfills, and smoking activities

were suggested as BC sources by Djossou et al. (2018). In the Niger delta of Nigeria, vehicle emissions in cities, bush burning in rural areas, and destruction of illicit local oil refineries, as well as gas flaring as part of oil processing, are all major sources of BC (Giwa et al., 2014; Oluleye and Folorunsho, 2020). As result, it could be said that the sources of BC could present significant regional dependence (Cui et al., 2021). The relationships between BC concentration and meteorological factors have also been assessed in many cities such as Mbour (Senegal), Accra (Ghana), Cotonou (Benin), Abidjan (Ivory Coast), Kwadela (South Africa) (Rivellini et al., 2017; Djossou et al., 2018; Xulu et al., 2020; Alli et al., 2021). The authors of these studies indicated that meteorological parameters including wind speed, temperature, relative humidity, and boundary layer height have an impact on BC concentrations in urban environments and that these factors vary on a diurnal and seasonal timescale.

In this study, attempts were performed to understand the long-term concentration variability of equivalent black carbon (eBC) mass concentration with state-of-the-art technologies in a North African urban area, Kenitra in the West region of Morocco. Online measurements of BC were conducted between mid-July 2020 to mid-February 2021 to investigate their long-term evolution, seasonal variation, meteorological effects, and emission sources. Using data acquired by a 7-wavelength aethalometer over a lengthy period, the objectives of this study are i) assessment of eBC mass concentration variability (daily, monthly, and seasonally), ii) determination of levels, and sources of BC and major factors influencing its variability, iii) comparison of BC levels among urban African and European areas, iv) creation of the first real-time database of BC within a typical North-African city, Kenitra, as there is currently no dataset available. To the best of the authors' knowledge, no long-term investigation of carbonaceous aerosols in North Africa has been reported utilizing online measurement techniques.

2. Materials and Methods

2.1 Instrumentation and sampling

A seven-wavelength (370, 470, 520, 590, 660, 880, and 950 nm) aethalometer (Model AE-31, Magee Scientific, USA) was used to perform online light-transmission measurements through a filter tape. The output of the aethalometer at each wavelength is expressed as equivalent black carbon mass concentration (BC) (Bernardoni et al., 2021). Measurements were carried out at a time resolution of 5-minutes from mid-July 2020 to mid-February 2021 in Kenitra, Morocco (Figure 1), in an urban area (Lat: 34.234194; Lon: -6.614889). Aethalometer was attached to $PM_{2.5}$ size-selective cyclone inlet (BGI, model SCC-1.828) pre-segregated all aerosols larger than 2.5 µm from inflowing the instrument, requiring a flow rate of 5 L/min. The inlet was situated on a terraced roof containing the instrument, at a height of approximately 15 m above ground level. The Aethalometer was sampling under ambient conditions where drying of the aerosol stream was not performed. The lack of an active drying process led to operational relative humidity (RH) being somewhat lower than the ambient relative humidity due to slightly elevated instrument temperatures, especially during the night (Schmid et al., 2005). In our case, the average recorded temperature and relative humidity in the measuring room in summer were, respectively, 28 °C and 63 %. The calculated dew point temperature was within 20°C. Schmid et al. (2005) argued that the dependence of aethalometer-derived absorption coefficients on RH is not statistically significant, at least for RH between 40 and 80%.

The used aethalometer (AE-31) is based on the measurement of the optical properties of aerosols collected on a filter tape, over a short period. The aethalometer relies on measurements of transmission of light through the filter to obtain optical absorption coefficients (σ_{abs}, usually given as $M.m^{-1}$) at each wavelength and then equivalent black carbon (eBC) concentrations (Hansen, 2005). However, several studies (Wang et al, 2018; Collaud Coen et al., 2010) highlighted that aethalometer filter-based measurements exhibit three kinds of artifacts including filter loading, filter scattering, and scattering from the collected aerosols. The measurement biases caused by filter effects generate some uncertainty in BC measurements. Corrigan et al. (2006) reported an uncertainty ranging from only 5% up to 40% in absorption coefficients measured by an Aethalometer. Zanatta et al. (2016) proposed an uncertainty of

35% for absorption coefficients derived from the Aethalometer. Recently, Mousavi et al. (2018), in their study of BC using a seven-wavelength aethalometer, calculated the uncertainty in the BC concentration to be about 29%. Although several correction methods and algorithms have been established to correct for measurement biases, none of them are ideal and much additional information is required to use them. Backman et al. (2017) stated, for deriving an aethalometer correction factor, that the use of an additional collocated filter-based photometer measuring aerosol light absorption coefficients including Multi-Angle Absorption Photometer (MAAP) and Particulate Soot Absorption Photometer (PSAP). However, Wang et al, (2018) reported that different corrected results for the same original data may be led by various suggested algorithms.

In this study, we used the uncorrected AE-31 multi-wavelength absorption obtained data to estimate the BC contributions. Ganguly et al., (2005) estimated that the filter-loading correction due to multiple scattering effects could be ignored within eBC mass concentration in the range of 2 - 4 $\mu g/m^3$. Ran et al. (2016) mentioned that measuring simultaneously and continuously aerosol absorption at different wavelengths has an important advantage. They suggested, to reduce systematic errors, handling properly multi-wavelength measurements that would be implied for exploring aerosol absorption spectral dependence, as well as inferring findings on chemical compositions and origins of light-absorbing aerosols.

Figure 1. Location of the measurement site of the Carbonaceous Aerosol in Kenitra (red square) located in the Atlantic region (upper right panel), far from the city centre of Kenitra (upper left panel), between three major traffic roads (bottom right panel), and in an urban area (bottom left panel). Note the different scales of the maps.

2.2 Data processing and analysis

2.2.1 eBC Concentrations:

According to the instrument manufacturer, the Equivalent Black Carbon (eBC) from aethalometer AE-31 was obtained from measurements at wavelength λ = 880 nm. eBC is the equivalent mass concentration of black carbon (BC) reported by the instrument. The eBC mass concentrations are

obtained by dividing the measured optical absorption coefficient (σ_{abs}) at each wavelength by a mass absorption cross-section (MAC, m^2/g). σ_{abs} is defined as the cross-section of carbonaceous aerosol available to absorb light per volume in which that eBC exists (Knox et al., 2009). MAC is wavelength-dependent which describes the eBC absorption per mass and scales inversely with wavelength. The eBC mass concentration from online measurements at the wavelength λ was obtained as follows (Eq. (1)):

$$\sigma_{abs}(M.m^{-1}) = eBC(\lambda) \text{x} MAC(m^2/g) \qquad (1)$$

In the AE-31, the MAC values are derived from $MAC(m^2/g) = \frac{14625}{\lambda}$, where λ is the wavelength in nm. By using the formula given by the manufacturer, the calculated value for the MAC at 880 nm is $16.62\ m^2/g$. The filter tape is automatically advanced when the maximum value of optical attenuation reaches a suggested threshold value of 80, so that readings can take place on a pristine spot. Although Petzold et al. (2013) advocated using the acronym eBC for reporting the black carbon mass obtained from the mass absorption cross-section, we use the abbreviation BC in this work as we are addressing black carbon in general and it is widely used.

The collected data during the mid-July 2020 to mid-February 2021 period are investigated in this study. Only collected data from the aethalometer between the 1st and 99th percentiles were retained and selected to calculate a valid aggregated value (hourly average) and subsequent calculations. Anomalous values including negative and occasional single extreme values were regarded as invalid, and less than 2% of data for Kenitra were discarded from the analysis. All the further averages, daily and monthly, were based on the >85% of validated hourly averaged data. Statistical data analyses were performed, comprising graphical presentations, in the base packages of the R programming language (R Core Team, 2020) and four of its additional libraries: openair (Carslaw and Ropkins, 2012), ggplot2 (Wickham, 2016), lubridate (Grolemund and Wickham, 2011) and dplyr (Wickham, 2021).

2.2.2 NO_2 and Meteorological data

Air quality pollutants (NO and NO_2) were monitored with 30-min time resolution at the same BC measurement site throughout the corresponding sampling period. Meteorological data records were obtained from the weather station Kenitra Airport (34.274°N, 6.569°W), about 6.3 km from our study site. The 6-hour meteorological data includes wind speed (WS), wind direction (WD), relative humidity (RH), air pressure (P), and air temperature (temp). Boundary layer height (BLH) was estimated using the HYSPLIT™ (Hybrid Single-Particle Lagrangian Integrated Trajectory model, Version 5.0) (Stein et al., 2015; Rolph et al., 2017) by running Meteorological Profile. The BLH data were retrieved from the GDAS (Global Data Assimilation System) one-degree archive with a resolution of 3 h, which has a time step of 3-hours and a horizontal grid spacing of 1° latitude by 1° longitude. The R package worldmet (Carslaw D., 2021) was used for accessing NOAA Integrated Surface Database (ISD) meteorological observations (NOAA, 2020). Half-hourly NO and NO_2 concentrations were continuously monitored onsite using a NO_x analyzer (HORIBA APNA-370). These auxiliary parameters were mainly used in correlation studies.

2.2.3 Backward Trajectory Analysis

To assess long-range transport patterns and explore the potential source regions contributing to the BC at the receptor site, the HYSPLIT™ (Version 5.0) was applied for air mass backward trajectory analyses (Benchrif et al., 2018; Jain et al., 2017). Air mass trajectories were provided by the GDAS current 7 days archive (ftp://arlftp.arlhq.noaa.gov/pub/archives/gdas1/, accessed on October 2021). The 48-hour backward trajectories at hourly intervals were plotted at an altitude of 500 m-agl throughout the observation period (four trajectories per day every 6 hours). The trajectory length is not related to the BC or aerosol lifetime, but to the reliability of the HYSPLIT model (Fossum et al., 2022). It can be limited to a certain duration since the associated HYSPLIT error in the trajectory calculation is proportional to 15-30% of the trajectory path length (Benchrif et al., 2018; Draxler and Rolph, 2007).

To characterize the regional sources of carbonaceous aerosol and the transport of air masses arriving at a sampling location, many studies (Botsa et al., 2021; Deng et al., 2020; Doumbia et al., 2012) used 120-hour runs for the backward trajectory analysis, while others (Sun et al., 2020a; Duc et al., 2020; Martinsson et al., 2017) calculated hourly backward trajectories for the past 48-72 hours. Different arrival heights (500, 800, and 1000 m-agl) of backward trajectories were tested and the results show that the transport pathways are not very sensitive to the chosen heights within the studied area. To group the back-trajectories into distinct transport patterns, the trajectory cluster analysis method based on the squared Euclidean distance metric was applied. Back-trajectory classifications based on cluster analysis allow much more detailed information about potential source regions affecting Kenitra city. It should be noted that we considered regional air masses as a proxy for long-range BC aerosol transport. In this study, the cluster analysis was performed on trajectories for the period of the experiment using a total of 812 back-trajectories. Seasonal variability is explored by clustering trajectories for each season individually.

3. Results and discussion

In the first section, we compare the average BC data measured in Kenitra city to similar data from other African and Worldwide cities with the purpose to assess the representativeness of the collected data with respect to the African continent, and to put our dataset into a broader perspective. Also, we briefly discuss the possible influence of COVID-19 restrictions. In the following section, we assess the meteorology of Kenitra during the studied period in comparison to the typical climatic conditions of Northern African coastal cities. Finally, we assess the temporal variability of BC in Kenitra, addressing the possible role of local sources and long-distance factors.

3.1. Overview of eBC mass concentration over Africa

The purpose of this section is to compare the average BC data measured in Kenitra city to data from other African and Worldwide cities. This is summarized in Table 1. In the Kenitra area, BC concentration was calculated (from mid-July to mid-February) to be on average 0.90 ± 0.80 μg/m^3. During winter (December to mid-February), autumn (September to November), and summer (mid-July to August) seasons, the mean BC value was 1.30 ± 1.17 μg/m^3, 1.01 ± 0.69 μg/m^3, and 0.75 ± 0.58 μg/m^3, respectively. It may be pointed out from Table 1 that the levels of BC concentration are similar to those obtained at some African sites. For instance, the BC value of Kenitra is comparable to the mean BC obtained by Gatari et al. (2003) at a rural burning biomass site in Nanyuki, Kenya (0.7 ± 0.06 μg/m^3), and observed by Xulu et al. (2020) during periods of winter biomass burning (1.9 ± 0.6 μg/m^3) and summer solid-fuel combustion (0.7 ± 0.2 μg/m^3) at residential urban areas in Kwadela, South Africa. It may be seen also that the BC values in Kenitra are in the same range as those obtained at Bou Ismaïl (Algeria) coastal urban site (0.41 - 2.85 μg/m^3) during Sep. 2011- Jan. 2012 period (Khedidji et al., 2020). Nonetheless, the BC concentration values of our site are largely lower to values reported in the literature at other urban traffic locations in Morocco (Tetouan) ranging between 3.01 - 3.22 μg/m^3 as reported by Benchrif et al. (2018), and Africa namely: Abidjan (7.0 ± 2.6 μg/m^3) (Adon et al., 2020), Bamako (19.2 ± 8.9 μg/m^3), Cotonou (4.9 ± 3.9 μg/m^3) (Doumbia et al., 2012), and Nairobi (2.3 ± 0.3 μg/m^3) (Gatari et al., 2003). Average BC levels measured in this study are similar to the range of values reported in previous studies at urban background sites in Rome (1.0 ± 0.6 μg/m^3) (Costabile et al., 2015), Barcelona (1.7 ± 0.6 μg/m^3), Huelva (0.7 ± 0.4 μg/m^3), and North Kensington (1.9 ± 0.7 μg/m^3) (Reche et al., 2011). Wang et al. (2020) reported BC values of 6.0 ± 2.9 μg/m^3, from November to December 2019, in Xi'an, China (Urban/ Residential site). Annual average BC measurements in urban and suburban sites in Shanghai, China quantified by Peng et al. (2019) are to be 1.17 ± 0.61 μg/m^3 and 2.09 ± 0.97 μg/m^3, respectively, attributed to the higher local combustion emissions and regional long-range transport. With this comparison, we can underline that Kenitra city (Morocco, North Africa) has particularly low carbonaceous pollution levels when compared to other traffic areas (e.g. West Africa) and megacities (e.g. Europe).

Furthermore, it may be noted that BC measurements were made during the COVID-19 curfew imposed by the government starting on June 11, 2020, and remained in place until the end of the sampling. A detailed timeline of the mobility restrictions and relaxation measures that have been taken in Kenitra city during the Coronavirus time is briefed in Table S6. Accordingly, the low levels found in this study are most likely linked to the nationwide curfew (between 7 p.m. and 5 a.m. or 9 p.m. to 6 a.m.) imposed by authorities during the sampling period because of the COVID-19 circumstances. The curfew time period in this study might not be truly representative of situations during typical business hours. During this period, most of the activities took place during the daytime which affect Morocco as a whole and reflect the unusual life of the city. Indeed, the lack of clear weekend/weekend effects would be expected as a long night curfew period was established in Kenitra. Panda et al. (2021) pointed out that the imposition of a night curfew influences the BC concentrations in Bhubaneswar, India, and declined by ~47%. Kompalli et al., (2014a) argued that the impact of cut-off of sources owing to issues like night-curfew or national strikes is dramatically remarkable. They found that BC concentrations in Indian semi-urban areas dropped quickly to ~22% of the average concentrations that prevailed before a regional "strike-work" that halted all industrial activities and commercial road traffic for two days. Otherwise, following the COVID-19 lockdown stage, Xu et al. (2020) found that BC values in the Chinese city curbed down by 44%, from 2.30 to 1.29 µg/m3. Gogoi et al. (2021) as well reported that BC levels from pre-lockdown observations are reduced significantly (10%-40%) in several Indian locations, mainly over the regions where there are abundant non-transport fossil fuel emission sources (e.g. industries, thermal power plants) compared to the those where the transport sector makes a major contributor.

Table 1: Comparison between BC values measured in Kenitra and across African and worldwide cities, focusing on urban sites described as being impacted by traffic. The table covers the type of sites, study period, measurement techniques/methods, and the most noteworthy findings. The table is ordered according to BC mass concentration.

Location	Type of location	Study period	Measurement techniques/methods	BC mass concentration range, µg/m^3	Reference
Middle Atlas (AM5), Morocco	Remote high-altitude	Aug.- Dec. 2017	Thermal-optical transmittance technique (Sunset laboratory, USA) in PM10 samples.	0.17 ± 0.10	Deabji et al. (2021)
Mbour, Senegal	Coastal site located in the outskirts of the city	Mar.- Jun. 2015	7-wavelength Aethalometer (AE-33) equipped with a PM1 impactor inlet (BGI model SCC-0.732) and sampled at 5 L/min.	0.36 ± 0.37	Rivellini et al. (2017)
Nanyuki, Kenya	Rural	May-June 1999	A black smoke detector model FH 62 I-N (ESM Emberline, Erlangen, Germany) for measuring fine BC.	0.7 ± 0.06 (0.4-1.1)	Gatari et al. (2003)
Huelva, Spain	Urban background site influenced by industrial emissions	2009	Multi-angle absorption photometer (MAAP Thermo ESM Andersen Instrument) with PM10 inlet.	0.7 ± 0.4	Reche et al. (2011)
Kenitra, Morocco	Urban	July 2020 to February 2021	7-wavelength aethalometer (AE-31) with a PM2.5 inlet and a flow rate of 5 L/min.	0.90 ± 0.80 (winter: 1.30 ± 1.17 ; autumn: 1.01 ± 0.69 and summer: 0.75 ± 0.58)	This work
Rome, Italy	Suburban background	Dec. 2011 – Feb. 2012	A 3-wavelength particle soot absorption photometer (PSAP) and Nephelometer (Ecotech, mod.Aurora 3000) operated to measure the dry aerosol scattering coefficient at three wavelengths (450,520, 635 nm).	1.0 ± 0.6	Costabile et al. (2015)
Shanghai, China	Urban	Jun. 2016- Jun. 2017	7-wavelength aethalometer model AE31 from Magee Scientific with inlet cut-off size of 2.5 µm and operated at a flow rate of 5 L/min.	1.17 ± 0.61	Peng et al., 2019
Bou Ismaïl, Algeria	Coastal area	Sep. 2011 to Jan. 2012	Thermal-optical transmittance technique (Sunset laboratory, USA) in PM10 samples.	1.25 (0.41 - 2.85)	Khedidji et al. (2020)
Cotonou, Benin	Urban traffic	Feb. 2015-Mar. 2017	IMPROVE_A Temperature Protocol for Thermal/Optical Carbon Analysis (in PM2.5 aerosols).	1.5 ± 0.2	Djossou et al. (2018)
Barcelona, Spain	Urban background site in a city with dense traffic	2009	Multi-angle absorption photometer (MAAP Thermo ESM Andersen Instrument) with PM10 inlet.	1.7 ± 0.6	Reche et al. (2011)
Kwadela, South Africa	Semi-Urban	Winter 2014 (Jul.-Sep.) and Summer 2015 (Feb.- Apr.)	Multiple wavelengths aethalometer (AE-22 and AE-31) with a PM2.5 inlet.	1.9 ± 0.6 (winter, AE-22) 0.7 ± 0.2 (summer, AE-31)	Xulu et al. (2020)
North Kensington, UK	Urban Background	2009	Magee AE-21 Aethalometer	1.9 ± 0.7	Reche et al. (2011)
Shanghai, China	Suburban	Jun. 2016- Jun. 2017	7-wavelength aethalometer model AE31 from Magee Scientific with inlet cut-off size of 2.5 µm and operated at a flow rate of 5 L/min.	2.09 ± 0.97	Peng et al., 2019

Hangzhou, China	Urban, Urban industry, Suburban, and Rural	1 Jan. - 31 Mar. 2020 (during, pre- and post-COVID-19 lockdown)	7-wavelength aethalometer (AE-31) with a flow rate of 5 L/min.	The citywide BC concentrations decrease from 2.30 to 1.29 µg/m3	Xu et al. (2020)
Nairobi, Kenya	Urban	March 2000	A black smoke detector model FH 62 I-N (ESM Emberline, Erlangen, Germany).	2.3 ± 0.3	Gatari et al. (2003)
Rome, Italy	Urban background	February 2017	7-wavelength aethalometer (AE-33) and Multi-Angle Absorption Photometer (MAAP).	2.6 ± 2.5	Costabile et al. (2017)
Tetouan, Morocco	Urban	May 2011 – Apr. 2012	A two-step combustion approach in PM2.5 developed by Cachier et al. (1989).	3.01-3.22	Benchrif et al. (2018)
Cotonou. Benin	Urban traffic	May 2005	7-wavelength aethalometer (AE-42) with a PM2.5 inlet and operated at a flow rate of 4 L/min.	4.9 ± 3.9	Doumbia et al. (2012)
Yaounde. Cameroon	Urban traffic	Aug. 2010	7-wavelength aethalometer (AE-31) with a PM2.5 inlet and a flow rate of 5 L/min.	5.7 ± 2.3	Doumbia et al. (2012)
Dakar, Senegal	Urban traffic	Jun. 08- Jul. 09	7-wavelength aethalometer (AE-42) with PM2.5 inlet and operated at a flow rate of 2 L/min.	5.7-15.4	Doumbia et al. (2012)
Xi'an, China	Urban/ Residential	1 Nov. - 31 Dec. 2019	7-wavelength aethalometer (AE-33) with PM2.5 inlet.	6.0 ± 2.9	Wang et al. (2020)
Abidjan, Ivory Coast	Urban traffic	Jan. 2016	Two-step thermal method in PM2.5 developed by Cachier et al. (1989).	7.0 ± 2.6	Adon et al., (2020)
Abidjan, Ivory Coast	Urban traffic	Feb. 2015-Mar. 2017	IMPROVE_A Temperature Protocol for Thermal/Optical Carbon Analysis (in PM2.5 aerosols).	7 ± 4	Djossou et al. (2018)
Addis Ababa, Ethiopia	Urban/ Residential	Nov.2015- Nov. 2016	Thermal-optical transmittance technique (Sunset laboratory, Forest Grove, OR, USA) in PM2.5 samples.	13.7 ± 6.8	Tefera et al., (2020)
Bamako. Mali	Urban traffic	April 2008	7-wavelength aethalometer (AE-42) with a PM2.5 inlet and operated at a flow rate of 4 L/min.	19.2 ± 8.9	Doumbia et al. (2012)

3.2 Meteorological situation

The meteorology of Kenitra (Table 2) is characterized by high temperatures in summer (mid-July to August), with monthly values ranging 37.1-13.0 °C, against 21.1-2.7 °C in winter (December to mid-February). Relative humidity stands between 75 % in summer, up to 79 % in autumn (September to November), and winter. Kenitra is usually windy, with wind speed averaging 2.7 m/s in autumn and winter, while it represents 3.3 m/s on average during summer. This is typical of North African cities which have semiarid and arid desert climates characterized by extremes in daily high and low temperatures, hot summers and cold winters, and minimal rainfall of approximately 200 to 400 mm per year for semi-arid regions and less than 100 mm per year for desert regions (NIC special report, 2009).

The time-series variations of temperature, rainfall, wind speed, air pressure, relative humidity, and boundary layer height derived from hourly measurements for the whole sampling period are shown in Figures S1a and S1b. The temperature variations show a decreasing trend from autumn to winter while the wind speed displays an increase including several episodes of stronger winds predominantly during the transition period (December-January). The seasonal cycle reveals that winter is associated with more stable atmospheric conditions due to lower wind speed compared to summer. Many episodes of rainfall and high relative humidity (>79 %) were very frequent during autumn and winter, particularly from December to January. The prevalent wind direction was the Southwest during the measurement campaign, while the Northwest prevailing wind direction was also registered. Higher frequencies of stronger winds (4–6 m/s and 6–8 m/s) were recorded during the autumn period. The wind rose (Figures 2 and S3) shows clearly that measurements were influenced dominantly by a fairly weak wind flow of 2.9 m/s on average from predominant west-southwestern directions. Winds from other directions are rarer. The air pressure ranged from 1002 to 1030 hPa, exhibiting an increase from summer to winter. A decreasing tendency was observed from mid-December to mid-January, with fluctuations in autumn. BLH ranged from 933.3 m in August to 953.1 m in December, with an annual average of 956.8 ± 165.3 m.

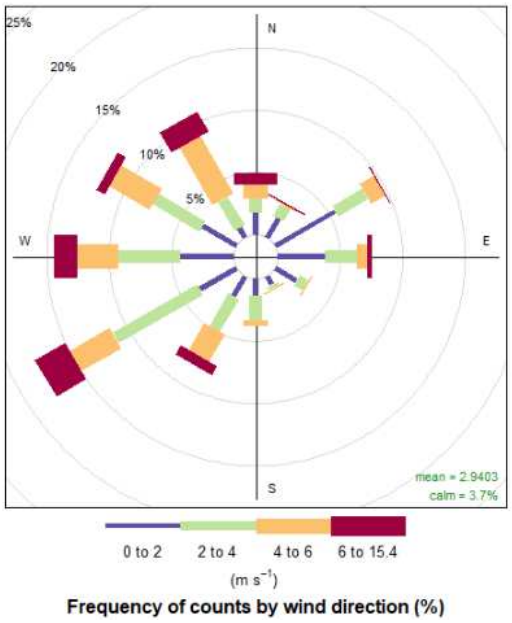

Figure 2: Wind rose based on hourly averages of wind speed and wind direction.

3.3 Seasonal features of BC concentrations at Kenitra

This section summarizes the BC concentration patterns from continuous measurements for eight months at Kenitra city. The corresponding monthly profile is shown in Figure 3 and descriptive statistics can be found in Table 2. As shown in Figure 3 and Table 2, the BC concentrations displayed a remarkable seasonal pattern, as their levels were high during winter and low during summer. The average (±SD, standard deviation) of BC concentrations were, respectively, 1298.1 ± 1169.3 ng/m^3 in winter (45% higher than the entire period average of 896.9 ± 800.3 ng/m^3), against 1006.0 ± 688.4 ng/m^3 (12% higher) in autumn and 752.1 ± 575.5 ng/m^3 (16% lower) during summer. The shape and trend of the seasonal variation of BC concentration are consistent with findings of Xulu et al. (2020) in Kwadela Township in South Africa and Doumbia et al. (2012) over Dakar city in Senegal. Several hypotheses are discussed below to explain the significant seasonal and monthly variation in BC concentrations.

Cao et al. (2009) argued that wind speed, wind direction, and temperature were important meteorological factors that affected BC concentrations. In our case study, however, a weak positive and negative association was revealed between BC and meteorological parameters, and the BC concentration variation was likely less affected by changes in this prevailing meteorology. Thus, our data were separated into three parts according to the season and conducted a correlation analysis in each of these seasons. Tables S2, S3, S4, and S5 provide a summary of the correlation matrices for the whole study period, and during the different seasons. The normality of the studied variables was checked using the Shapiro-Wilk test, which showed all variables don't follow the normal distribution. Then, Spearman correlations were employed. The calculated Spearman's correlation coefficients indicated that carbonaceous fraction concentrations are significantly correlated with meteorological factors, at 95% or 99% confidence levels. As shown, the relation between BC and WS, RH, T, and P varies with the seasons, and the correlation in winter is slightly stronger than in summer and autumn. For instance, a weak negative correlation between BC concentrations and wind speed was found (r ranged from -0.46 ($p<0.01$) in winter to -0.31 ($p<0.01$) in autumn and -0.23 ($p<0.01$) in summer). These results support the fact that seasonal variations do exist in the relationships between BC concentrations and meteorological factors. In addition, the BC concentration throughout winter was likely driven primarily by the low wind speed, confirming the key role of wind speed, among other meteorological factors in the observed BC concentrations (Sun et al, 2020b). The seasonal variation in BC mass concentration could also be mainly related to seasonal differences in BLH as well as meteorological factors. The observed stable BLH, due to the low wind speed and hence low surface convection, prevents aerosol particles from dispersing

strongly into the atmosphere and is enclosed near the boundary layer showing the high BC concentration in winter (Guha et al., 2014). In general, the atmosphere of Kenitra during the winter season is characterized by high relative humidity and low ventilation coefficients, leading to lower aerosol dispersion and, as a result, an increase in BC concentrations. However, the decrease in BC from winter to summer can be related to the combined effects including the increase in ventilation coefficient (the product of BLH height and wind speed) in the hot season (Beegum et al., 2009; Kompalli et al., 2014b). During the summer season, the enhancement of both BLH and ventilation coefficient are conducive conditions for lofting on near-surface aerosols to higher atmospheric levels. Aside from these former, the local emissions and long-distance aerosol transport also contribute to the seasonal differences, which are discussed in subsequent paragraphs.

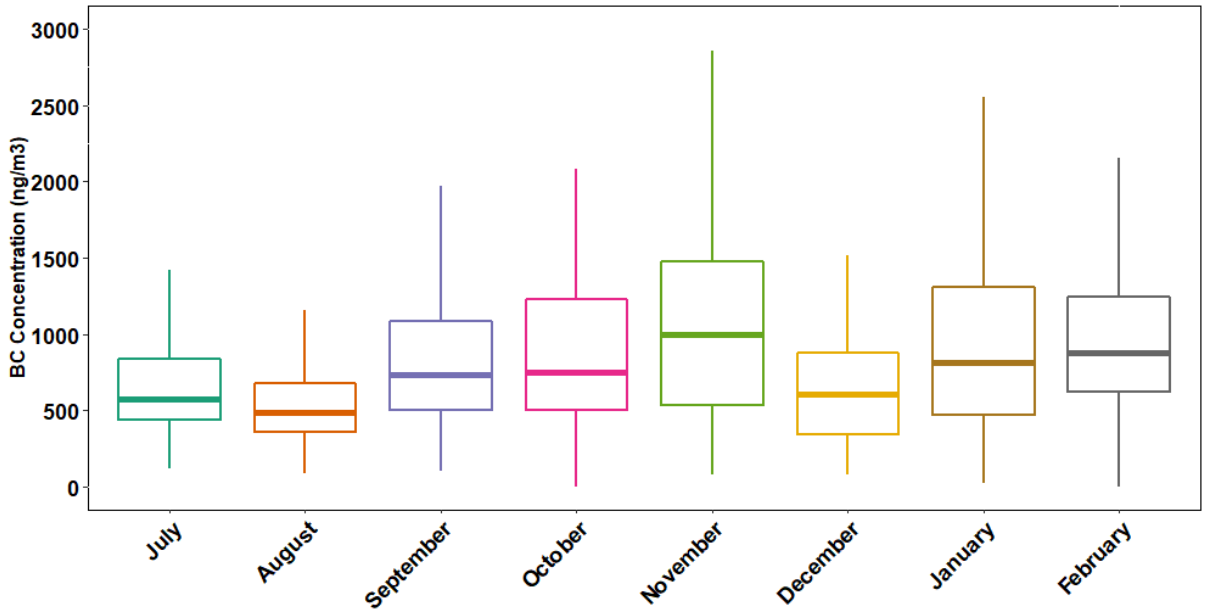

Figure 3: Monthly profile of BC measured at 880 nm in Kenitra city between July 2020 and February 2021. Box-plot indicates minimum, maximum, median (dash line), and 25/75% quartiles (boxes) in the dataset. Descriptive statistics of monthly BC concentrations are summarized in Table S1. It is worth noting that because of the failure of the instrument system, a remarkable decline in BC levels is observed in December due to the reduction in the number of valid observations as shown in Table S1.

Correlation analysis of BC with NO, NO_2, and NO_x (Figure S4) shows that the relationship between BC and NO_2 followed two different patterns. The mass concentrations of BC were good correlated with the NO_2 concentrations during the cold season as on November 2020 ($r=0.67$, p-value < 5.194e-11 which is less than the significance level $\alpha=0.05$) and January 2021, ($r=0.57$, p-value < 2.2e-16), but a weaker correlation ($r=0.49$, p-value < 1.851e-09) was found for the other sampling days (August 2020). It can be inferred that these are the results of the increase in traffic-related pollutants in the winter. Increased traffic activities can result in increased emissions of NO_2 and other air pollutants. Accordingly, we can speculate that the increase in NO_2 levels makes the correlation between BC concentrations and some meteorological factors stronger.

Another hypothesis involves that the observed BC variations are probably due to the changes in regional and long-range emission sources as discussed by Doumbia et al. (2012) and Pani et al. (2020). Accordingly and to identify different source regions that are likely to impact BC levels in Kenitra city, the cluster analysis technique based on the squared Euclidean distance metric was applied to HYSPLIT back-trajectories of air masses arriving at the sampling site. Figure 4a shows mean back-trajectories arriving at Kenitra from mid-July 2020 to mid-February 2021 classified into 6 backward trajectory clusters. The major transport patterns can be summarized as follow: Slow North-easterly (24.0% of the

time, cluster (or C) 1), North-westerly (57.1%, C2, 3, and 4), and South-westerly (15.5%, C5 and 6). As shown in Figure 4b, the air masses from the Western coast of Morocco (C6) remain below 800 m for 48 hours before reaching Kenitra. The air masses from northern regions of Morocco (C1) travel at altitudes between 600 and 800 m for the last 24 h until they approach Kenitra. On the contrary, the air masses from the Atlantic Ocean (C5 and C4) travel above 800 m in altitude most of the time. The clusters (C5 and C6) display different transport elevation profiles although air masses followed the same path the day before reaching the sampling site.

Several studies (Lack et al., 2012 and Mamoudou et al., 2018) stated that BC emissions from international ships are very significant. Jonson et al. (2020) reported that in addition to NO_2 and sulfur considered as the main sources of particles from shipping, it is assumed that BC is also emitted as primary particles. Cui et al. (2021) confirmed that regional transports have a significant impact on BC levels. They found that long-range aerosol transport, especially when air masses were linked to regions with high ship emissions as in the Yellow Sea and the Bohai Sea, could not be negligible for contributing to BC pollution in rural Qingdao, north-eastern China. A key characteristic of backward trajectory clusters classification is that the contribution of long-range carried aerosols outside areas is combined with primary emissions of carbonaceous components released by the maritime activity in the Atlantic region. These long-range contributions, however, are far from large enough to explain the observed seasonal variations in BC concentrations, as BC values are assumed to be the result of the contribution from the different source sectors, namely long-range and local emissions.

Figure 4c illustrates the back-trajectory analyses throughout different seasons of the sampling period. Contrary to the other seasons, the clustering of back-trajectories during winter led to distinct clusters (C1 and C4) corresponding to air masses within 500 m and relatively high concentrations of carbonaceous aerosols (Table 3). BC concentrations from C1 to C4 have comparable values of around 1.4 µg/m3. A high BC value (1.4 µg/m3) was measured in autumn, driven by the air masses from the West coast of Morocco (C3). The other autumn clusters, C1, C2, C4, and C5, also showed high BC levels, averaging 1.0-1.1 µg/m3. It is, therefore, reasonable to assume that the polluted air masses, during the last 24 h before reaching Kenitra, are likely to be a key feature affecting the BC concentrations and causing part of the pronounced seasonal variation are: i) slowly traveling from the West coast of Morocco over the populated areas of Casablanca towards Kenitra; and ii) coming from the near Atlantic Ocean, affected by pollutants emitted from Northern cities of Morocco and Gibraltar Straight. In conclusion, until this stage, the observed trend whereby BC concentration increases during winter and drops during summer can be explained by varying emission sources, meteorological conditions, and air masse trajectory height and pathways.

Using bivariate polar plots, by calculating the mean concentration for wind speed and directions bins, it was possible to identify and understand the sources of BC coming from different directions (Grange et al., 2016). These graphs show how the concentration of BC varies according to the speed and direction of the wind. In their simplest form, BC concentrations are aggregated into wind speed and wind direction bins and are displayed on polar coordinates. Figure 5 presents polar plots of BC concentration for the whole period (upper panel) and in three seasons (winter, summer, and autumn) at Kenitra city. It suggests that locally-sourced carbonaceous aerosol was present, as demonstrated by the elevated concentrations at low wind speeds, while the low concentrations were observed with westerly winds at high wind speeds (>8 m/s). In the winter, it was observed that high concentrations of BC come from everywhere, being more relevant from the east with weak winds with speeds ranging from 0 to 4 m/s. In the autumn, high BC concentrations come from the northwest associated with strong winds with speeds ranging from 3 to 7 m/s. By contrast, summer showed that only when wind speeds were high, moderate to low concentrations were experienced due to enough degree of pollutant dispersion. Concisely, polar plots indicated that the major source of BC is in the vicinity of the monitoring site, consistent with road traffic. Moreover, long-range south-westerly atmospheric transport events can contribute to elevated BC concentrations.

Table 2: Summary of the mean (± standard deviation), minimum (min), and maximum (max) concentrations of 5-minutes BC (i.e., total BC), Daily-Ratio (Ratio of hourly BC between night-time and daytime), and 6-hours meteorological parameters (T (temperature), P (pressure), BLH (Boundary layer height), RH (relative humidity), WD (wind direction) and WS (wind speed)) between mid-July 2020 to mid-February 2021 (203 days). Summary data are also subdivided into seasons over Kenitra city. n.a = not available. N stands for the number of total datasets used, where N = 11434 for BC; and N = 781 for meteorological parameters.

Variable	Entire period	Winter	Autumn	Summer
	Mean ± SD [Max - Min]			
N for BC	11434	2730	649	8055
BC (ng/m^3)	896.9 ± 800.3 [6693.0 - 0.7]	1298.1 ± 1169.3 [6693.0 - 0.7]	1006.0 ± 688.4 [4214.0 - 1.9]	752.1 ± 575.5 [6494.0 - 89.0]
Daily-Ratio of hourly BC	1.19 [1.37 - 0.74]	1.49 [1.78 - 1.07]	1.32 [1.80 - 0.88]	1.02 [1.29 - 0.52]
N for meteorological parameters	781.0	144	325	312
T (°C)	18.3 ± 6.0 [37.1- 2.7]	12.4 ± 4.0 [21.2 - 2.7]	16.2 ± 4.6 [29.5 - 4.0]	23.3 ± 3.9 [37.1 - 13.0]
RH (%)	79.2 ± 17.0 [100.0 - 0.0]	86.8 ± 16.1 [100.0 - 0.0]	79.0 ± 19.0 [100.0 - 0.0]	75.8 ± 13.8 [100.0 - 0.0]
BLH (m-agl)	956.8 ± 165.3 [1396.0 - 118.0]	946.8 ± 183.3 [1396.0 - 119.0]	960.9 ± 171.7 [1382.0 - 118.0]	956.1 ± 148.9 [1347.0 - 465.0]
WS (m/s)	2.9 ± 2.1 [15.4 - 0.0]	2.7 ± 2.1 [9.8 - 0.0]	2.7 ± 2.1 [15.4 - 0.0]	3.3 ± 1.9 [9.8 - 0.0]
WD (degree)	218.4 ± 100.4 [360.0 - 10.0]	168.5 ± 97.2 [360.0 - 10.0]	199.6 ± 105.6 [360.0 - 10.0]	261.7 ± 76.6 [360.0 - 10.0]
P (hPa)	1017.2 ± 5.03 [1030.5 - 1002.2]	1019.7 ± 6.9 [1030.5 - 1002.2]	1018.7 ± 4.3 [1027.7 - 1006.7]	1014.3 ± 2.9 [1023.4 - 1007.8]
Sunrise time (a.m, local time)	n.a	08:27 [08:33- 08:15]	07:34 [08:14 - 07:00]	06:42 [07:00 - 06:26]
Sunset time (p.m, local time)	n.a	06:33 [07:04 - 06:15]	06:53 [07:50 - 06:15]	08:17 [08:37 - 07:52]

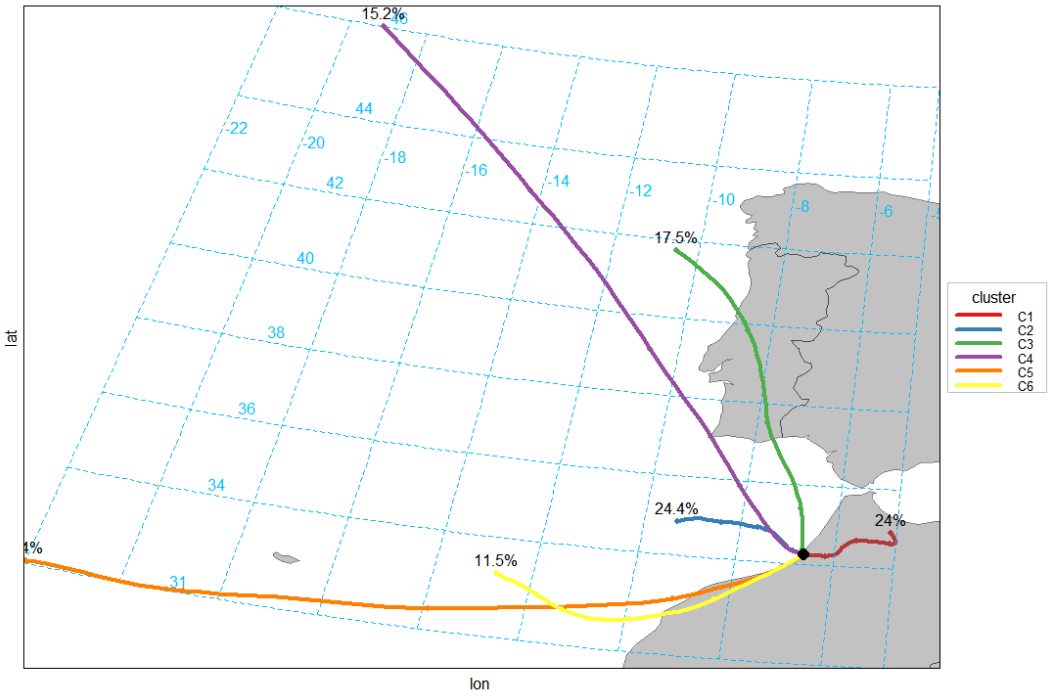

Figure 4a: mean back-trajectories arriving at Kenitra from mid-July 2020 to mid-February 2021 classified into 6 backward trajectory clusters.

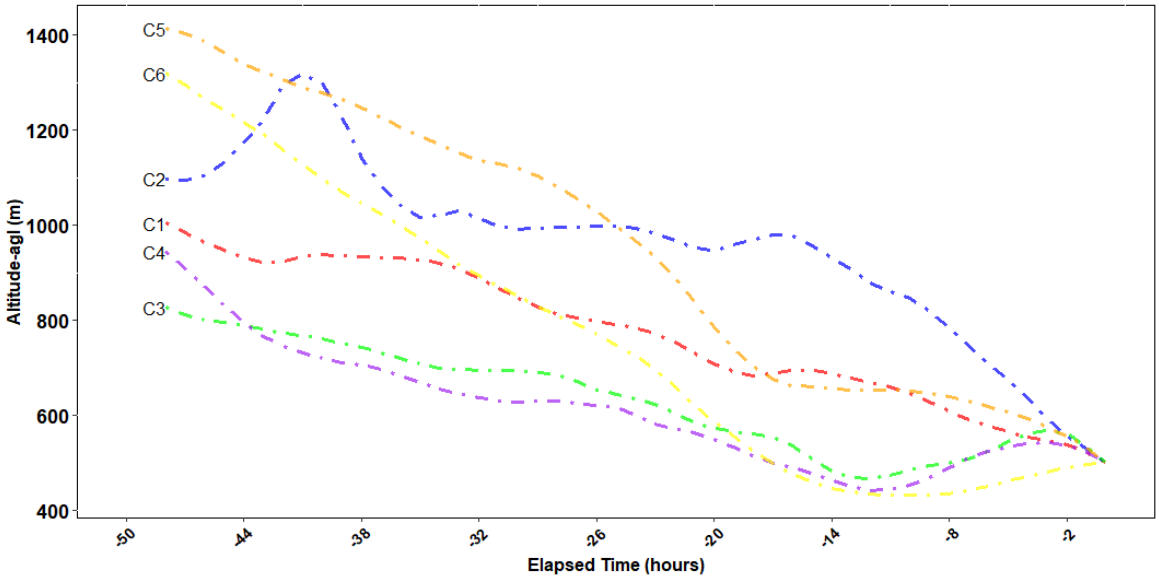

Figure 4b: Mean altitudes of each back-trajectory cluster during the whole period.

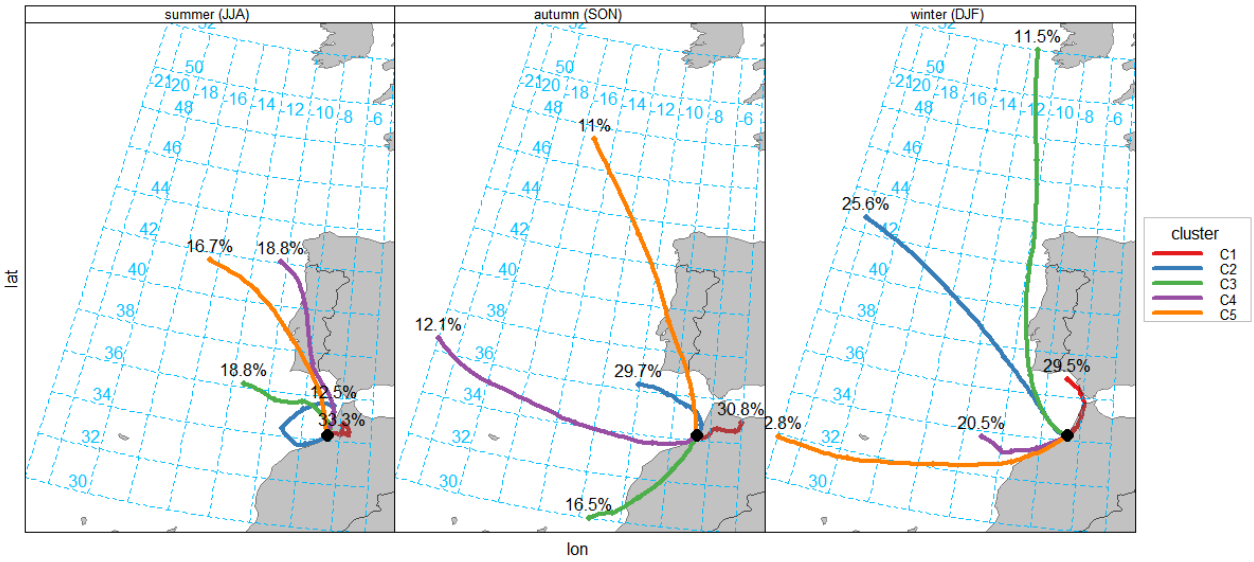

435

436 Figure 4c: Mean back-trajectories arriving at Kenitra from mid-July 2020 to mid-February 2021
437 classified into 6 backward trajectory clusters and subdivided into seasons: summer (from mid-July to
438 August), winter (from December to mid-February), and autumn (from September to November).

439 Table 3: Summary of the mean (± standard deviation), minimum (min), and maximum (max)
440 concentrations of BC related to the obtained clusters during the whole period and the three seasons. n.a
441 = not available.

Variable	Entire period	Winter	Autumn	Summer
BC (ng/m^3)	Mean±SD [Max - Min]			
N of Clusters	6	5	5	5
C1	989.2 ± 561.0 [2934.1 - 381.3]	1444.5 ± 958.7 [3100.8 - 554.0]	1035.4 ± 463.2 [2565.3 - 381.3]	567.8 ± 154.6 [989.3 - 397.4]
C2	1015.2 ± 624.1 [3421.6 - 416.6]	940.1 ± 305.2 [1445.2 - 562.1]	1043.6 ± 274.1 [1812.2 - 720.4]	630.8 ± 146.3 [864.5 - 416.6]
C3	926.5 ± 535.0 [3100.8 170.2]	475.8 ± 341.5 [950.7 - 170.2]	1446.2 ± 682.5 [2665.0 - 500.2]	627.3 ± 186.4 [968.6 - 458.6]
C4	928.8 ± 338.0 [1705.7 - 462.7]	1412.6 ± 1123.8 [3421.6 - 457.5]	1057.9 ± 189.9 [1312.3 - 654.7]	704.5 ± 241.6 [1145.9 - 448.2]
C5	894.6 ± 390.4 [1530.1 - 226.8]	798.8 ± 488.5 [1530.1 - 226.8]	1053.7 ± 367.3 [1705.7 - 462.7]	785.5 ± 136.3 [970.3 - 649.1]
C6	1211.9 ± 635.5 [2665.0 - 457.5]	n.a	n.a	n.a

442

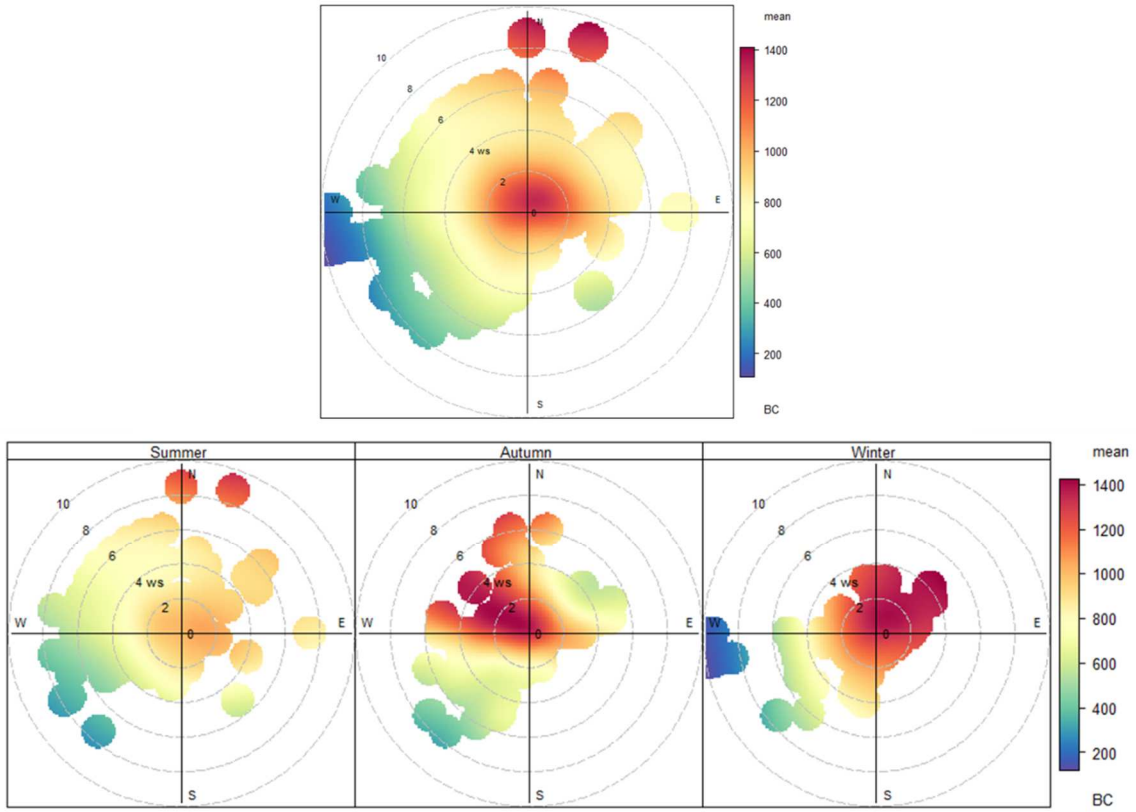

Figure 5: Polar Plots of BC concentration for the whole period (upper panel) and in three seasons (winter, summer, and autumn) at Kenitra city. The average of BC concentrations (ng/m^3) is coded as a colour scale shown to the right. The dashed circular grey lines show the wind speed scale.

3.4 Diurnal BC concentrations patterns

Besides the seasonal averages, the profile of BC concentration has also been evaluated on a higher temporal resolution. Diurnal cycles of BC have been calculated as 1-hour mean values and are shown in Figures 6a and 6b. From the temporal variation plots of hourly-averaged BC concentrations, a well-defined and significant diurnal variation was observed throughout the day. Overall, a steady build-up in the BC concentration to sharp peaks between 06:00 and 09:00 a.m local time (LT) just after sunrise preceded by a smooth decrease to low concentration at midday (11:00 a.m - 05:00 p.m) and then again starts increasing to attain another peak value at evening around 09:00 p.m after sunset. Table 2 shows the sunrise and sunset time in different seasons. During the whole period, mean hourly BC concentrations were found to range between 571.7 and 1311.6 ng/m^3 with an average value of 908.8 ng/m^3. In summer, the average diurnal profile was fairly flat, with a sharp peak in the morning centered on 06:00 to 09:00 a.m, accompanied by decreasing trend to minimum values reached at about 03:00 to 04:00 p.m, and then followed by gradual ascending with broader evening peak appeared at 09:00 p.m. The BC level was still maintained until midnight. The average hourly BC concentration during summer is 758.1 ng/m^3 and ranged from 516.9 to 1365.6 ng/m^3. During winter, the average diurnal profile showed a pre-dawn minimum at 5:00 a.m followed by a wide peak in the morning from 6:00 a.m to 12:00 p.m and a second peak, relatively more pronounced, during 06:00-11:00 p.m. The BC concentration during the night-time followed an increasing pattern until 02:00 a.m, and the maximum mean concentration exceeded nearly 2000 ng/m^3. Maximum hourly BC concentrations in the morning were about 1365.6 (at 07:00 a.m), 1432.9 (at 08:00 a.m), and 1548.3 ng/m^3 (at 10:00 a.m), and at evening were around 952.1 (at 09:00 p.m), 1482.7 (at 11:00 p.m) and 2004.7 ng/m^3 (at 10:00 p.m) during summer, autumn, and winter, respectively.

These indicate that the highest values were found during the winter and the lowest values were obtained during the summer, which is consistent with the seasonal changes previously discussed. The diurnal amplitudes (ratio of night-time peak to the daily minimum) of BC values were found to be seasonally dependent with the maximum occurring in winter (~3.1), followed by autumn (~2.4), and the lowest values observed during summer (~1.8). The mean annual variation amplitude of ~ 2.0 is of the order of magnitude observed in semi-urban Nagpur, Central India (Kompalli et al., 2014b). Hourly changes in BC concentrations throughout the autumn season indicated also bimodal distributions alike winter and summer seasons, while they were found to be the smallest during midday. The ratios of BC concentrations between winter and summer exhibit that the winter BC level is about a factor of 1.5 - 2.7 higher than those measured in summer during the morning and of 2.2 - 2.9 during the late evening. During the afternoon hours, this ratio increases to about 2.8 to 4.0. The striking feature is that the average ratio between night-time (07:00 p.m to 06:00 a.m) and daytime (07:00 a.m to 06:00 p.m) of BC concentrations, estimated during the whole period, was found to be larger than the unity (1.19) as shown in Table 2. However, this feature is not pronounced during evening hours (06:00 - 08:00 p.m) when BC concentrations observed are lower than in the morning, excepting the winter season (ratio = 1.37). Tiwari et al. (2013) suggested that ratios larger than the unity are likely to indicate that the evening peaks result from changes in emission sources and variability in meteorological conditions. Doumbia et al. (2012) advocated that this may be attributed to the strong contribution of local sources mainly commuter traffic and to the fumigation effect in the boundary layer, which brings the evening aerosols near the surface from the nocturnal residual boundary layer shortly after the sunrise. Srivastava et al. (2019) stated that the entrainment of nocturnal BC residues begins in the early hours of the morning and leads to an increased BC concentration for a few hours. This phenomenon, commonly referred to as the fumigation effect, coupled with other anthropogenic emissions during early rush hours, is likely responsible for the morning BC peaks. Season-wise, its ratio was found to be 1.49, 1.32, and 1.02 during the winter, autumn, and summer seasons, respectively, exhibiting certain seasonal differences, which may be attributed to the differences in emission intensity and meteorological conditions of the sources associated with BC in each season. The most noticeable feature is that most of the time, the morning BC concentrations are higher than those observed during the evening hours. These BC diurnal profile peaks observed in this study were very comparable to that documented by others at different locations as in Shenzhen by Sun et al. (2020b), Karachi by Bibi et al. (2017), Dakar and Bamako by Doumbia et al. (2012), New Delhi by Tiwari et al. (2013), and Pune by Safai et al. (2007), i.e., distinct seasonal hourly BC trends can be noticed throughout the entire day (winter>autumn>summer). In a summary, it was observed that the diurnal profile of BC concentration follows bimodal behaviour in all the seasons but with varying degrees of the magnitude of the peaks. Indeed, the striking feature is that the morning peaks were more pronounced as compared with evening ones, and peaks were highest in winter and lowest in summer.

The fumigation effect leads to morning peaks in BC concentrations. The thermals generated after sunrise break the night-time inversion and bring down the BC from the residual layer to the surface, resulting in a peak. Concentration in rush hour traffic due to the build-up of vehicle traffic also contributes to this. Following this, enhanced convective mixing together with a deepening of the BLH leads to a drop in BC concentrations at the surface. As the thermals subside after sunset, the shallow nocturnal boundary layer sets in and the resulting stable conditions result in BC confinement near the surface. In addition, typically lower temperatures and wind speeds coupled with reduced source strength (less traffic during night-time curfews) lead to a gradual decrease in BC mass concentration leading to a night-time minimum. Seasonal differences in fumigation amplitudes and nocturnal BC peaks are driven by reduced source strengths and the evolution of BLH.

Over Kenitra, the BC concentration variations matched well with variations in diurnal anthropogenic activity emissions, population living style, and boundary layer development. Several studies (Liu et al., 2020; Tiwari et al., 2013; Doumbia et al., 2012; Safai et al., 2007) stated that the relationship between the BC concentrations and boundary layer height exhibits a negative correlation where the increased BC levels resulted in the lower boundary layer height. Ramachandran and Rajesh (2007) reported that the nocturnal boundary layer is three times narrower than that during daytime. Morning and evening BC peaks are likely driven primarily by anthropogenic activities (i.e. biomass burning, industrial activities, vehicular emission) and low boundary layer height during the morning and evening hours. Accordingly,

both increased local traffic emissions and the nocturnal boundary layer brake, which lifts aerosols to the surface shortly after sunrise, contributed to the morning peaks. At noon hours, low BC concentrations are attributed to i) aerosol dispersion due to the increase in surface temperatures which causes convective activity (i.e., mixing) and elevation of the boundary layer (i.e., dilution), and ii) gradual decrease in traffic volume after the morning rush hour. Later, the BC concentrations started building up gradually and evening peaks started reappearing due to the commuter traffic activities (back home) that occurred during this time and the decadence of the boundary layer. Ezani et al. (2021) argued that at sunset both the boundary layer decreases and the atmospheric stability increases may lead to BC concentrations increasing again. Then after, as shown in Figures 6a and 6b, the BC concentrations went on decreasing slowly during the night-time but the BC levels were high which can be partly explained by trucks and freight traffic either on the national way or the highway. As shown in Figure 1, the sampling site is surrounded by three major traffic roads with distances between the site and these highways/corridors ranging from 2.6 to 3.7 Km. As trucks typically have higher emission factors, which, when combined with the general shadow boundary layer height during the evening leads to the enrichment of BC near the surface (i.e. the evening peak) (Sun et al., 2020b). In brief, the observed diurnal variation of BC concentrations is mainly attributed to the dynamics of the boundary layer height, although the urban and local traffic activities might be contributing to the morning and nocturnal peaks.

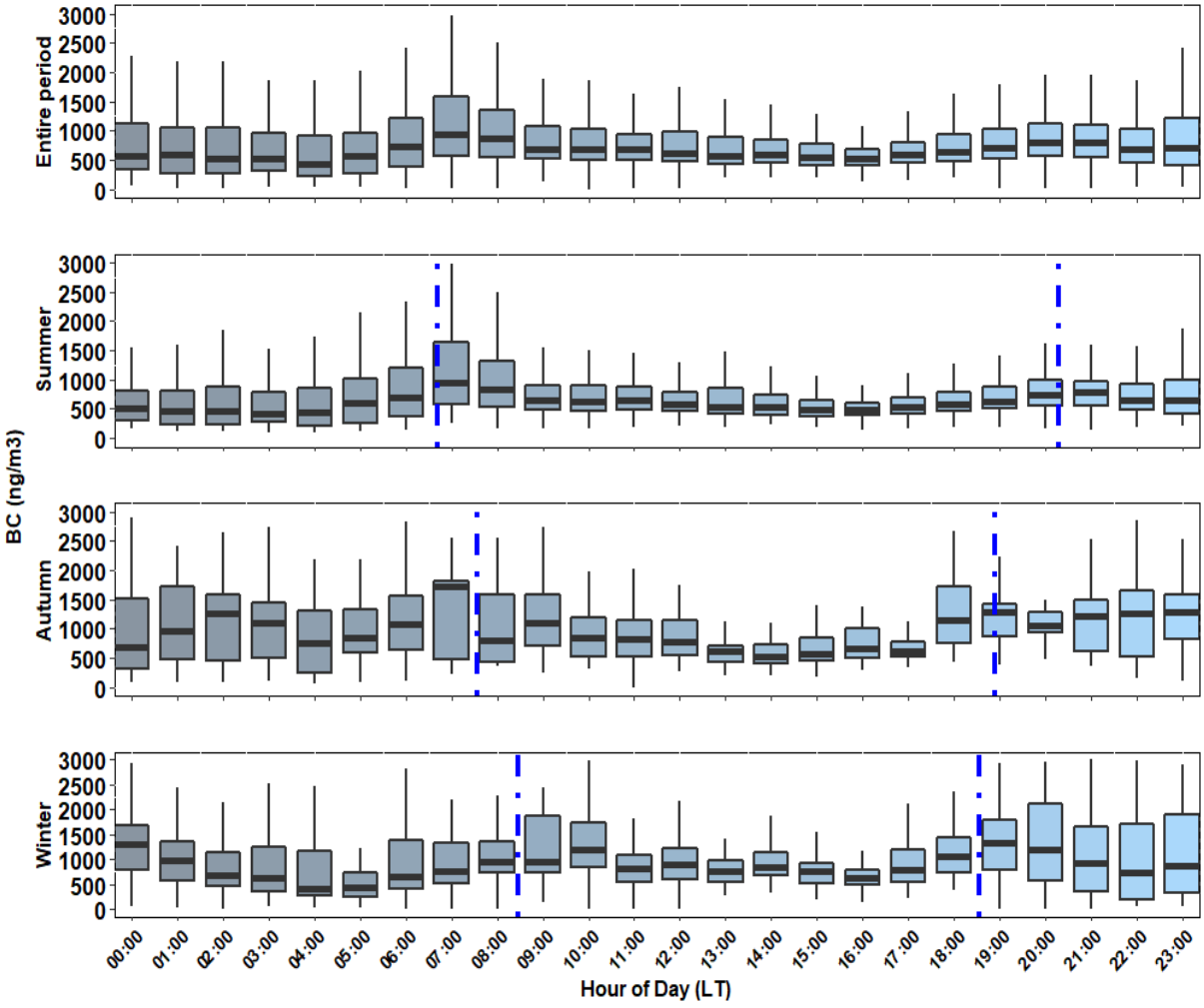

Figure 6a: The diurnal distribution of BC during summer (mid-July - August), winter (December – mid-February), and autumn (September - November) seasons, and the whole sampling period (upper panel). The horizontal lines represent the medians; the limits of the boxes are the 1st and 3rd quartiles. The whiskers extend to one and a half times the interquartile range. Dotted vertical lines represent the seasonally mean sunrise and sunset times. Hours are in local time, LT.

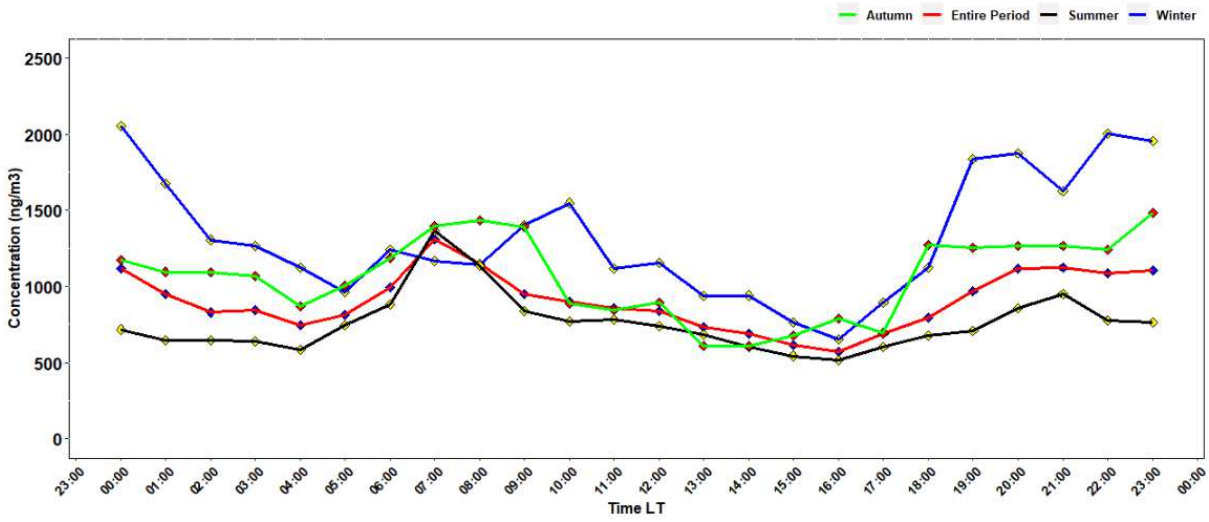

Figure 6b: Hourly changes in BC concentrations throughout summer, winter, and autumn seasons. Plotted points are the average values for aggregated data from the subsequent one hour on available days (e.g., 10:00 LT represents the time from 10:00 LT to 10:59 LT). LT stands for local time.

4. Future outlook

This study aims at providing insights into an open gap in the scientific community, which is the spatial variability of the black carbon aerosol in different environments and at different sites. We provide novel data from North Africa (Morocco), with an emphasis on particular local conditions that multiply the BC concentrations and consequently can affect human health. We finally participate in research efforts to monitor carbonaceous aerosol emissions to inform the public of potential exposure.

This study is expected to provide valuable information to understand BC levels in North African urban areas, relevant temporal variability, and emission sources and put this data into a larger perspective. It also offers a reference for future attempts to assess fine carbonaceous aerosols in urban African areas. Future outlook studies should concentrate on the role of local anthropogenic activities as compared to long-range transport, and in particular on the impact of changes in regional characteristics on BC concentrations in the Mediterranean areas; and BC source apportionment into wood burning (WB) and fossil fuel combustion (FF) to investigate the quantitative contribution of such non-traffic sources to BC (manuscript in preparation, comparing data between Kenitra, Morocco and Rome, Italy).

Limitations of this study include the sample size and non-uniform data spans, and these cannot be changed due to variations in observational records. Future studies should add by performing longer (i.e., at least one-year) period characterization and trend analysis of BC concentrations, and using our data as reference for previously available and valid observations.

5. Conclusion

The findings of this study provide the first attempt to assess long-term BC levels with state-of-the-art technologies at a North-African urban area, Kenitra, in western Morocco. Data were collected during mi-July 2020 - mi-February 2021. Based on average BC levels in the last 10 years, Kenitra represents a low-to-medium BC concentration urban area for Africa, where data as high as more the 6 times were found. Whether this is due to the peculiar COVID-19 period, different emission sources, or the different measurement methods used will be the subject of future research.

In addition to these previous studies, the continuous dataset collected in this work with higher time resolution (5-minutes continuous data for almost one year vs. 24-hours sporadic measurements) shed

light on diurnal, monthly, and seasonal variability in BC mass concentration over this African urban location (Kenitra).

The major findings obtained are summarized as follows:

- The average BC concentration observed in this study (0.90 ± 0.80 µg/m^3) is overall lower than those reported in African and European urban locations. This observed low carbonaceous pollution levels may be partially attributed to the reduction of anthropogenic activities due to the COVID19 curfew imposed by the authorities.
- BC concentrations displayed a clear bimodal diurnal pattern, in which morning peaks were attributed to morning inversion and rush-hour traffic, while evening peaks were related to combustion sources (evening traffic rush-hour) and the impacts of a shallow night-time boundary layer.
- The average BC values at night-time (07:00 p.m to 06:00 a.m) are 1.9 times greater than those observed throughout the day (07:00 a.m to 06:00 p.m) as the atmospheric boundary layer is shallower at night, retaining pollutants in a smaller volume, which leads to higher BC mass concentrations.
- BC exhibits a strong seasonal variability, ranging from a low of 0.75 µg/m^3 in the summer to a high of 1.30 µg/m^3 in the winter. Although lower BC concentration occurs in the summer due to aerosol dispersion driven by high wind speed, higher BC arises during winter due to shallow atmospheric boundary layer, long-range transport, and local emissions associated with low wind speeds.
- The association of BC with low wind speeds without marked directionality is a clear indication that the major source of BC is in the vicinity of the monitoring site, consistent with road traffic. Moreover, long-range westerly atmospheric transport events can contribute to elevated BC concentrations.
- During the afternoon period (11:00 a.m - 04:00 p.m), the BC concentration values are minimum (do not exceed the value of 500 ng/m^3, on average), because of the fully evolved boundary layer and reduced traffic activities, representing somehow an urban background level in Kenitra.

Author contributions

Youssef Bounakhla: Performing the experiment, Writing - original draft preparation. Abdelfettah Benchrif: Conceptualization, Data Analysis, Writing - original draft, Supervision. Mounia Tahri: Writing - review & editing. Francesca Costabile: Conceptualization, Writing - review & editing. Fatiha Zahry: Performing the experiment. Moussa Bounakhla: Supervision. El Kafssaoui El Hassan: Supervision. All authors have read and agreed to the published version of the manuscript.

Competing interests

The authors declare that they have no conflict of interest.

Acknowledgments

The authors gratefully acknowledge the financial support from the bilateral CNRST (Morocco)-CNR (Italy) cooperation framework (Research Contract N° 7/2020 PICS Italy). They also acknowledge the NOAA Air Resources Laboratory (ARL) for the provision of the HYSPLIT transport and dispersion model used in this publication.

5. References:

Adon, A.J., Liousse, C., Doumbia, E.H., Baeza-Squiban, A., Cachier, H., Léon, J.F., Yoboué, V., Akpo, A.B., Galy-Lacaux, C., Guinot, B., Zouiten, C., Xu, H., Gardrat, E., & Keita, S. (2020). Physico-

chemical characterization of urban aerosols from specific combustion sources in West Africa at Abidjan in Côte d'Ivoire and Cotonou in Benin in the frame of the DACCIWA program. Atmospheric Chemistry and Physics, 20, 5327-5354. DOI:10.5194/ACP-20-5327-2020.

Alli, A.S., Clark, S.N., Hughes, A., Nimo, J., Bedford-Moses, J., Baah, S., Wang, J., Vallarino, J.A., Agyemang, E., Barratt, B., Beddows, A.V., Kelly, F.J., Owusu, G., Baumgartner, J., Brauer, M., Ezzati, M., Agyei-Mensah, S., & Arku, R.E. (2021). Spatial-temporal patterns of ambient fine particulate matter (PM2.5) and black carbon (BC) pollution in Accra. Environmental Research Letters, 16. DOI:10.1088/1748-9326/ac074a.

Backman, J., Schmeisser, L., Virkkula, A., Ogren, J.A., Asmi, E., Starkweather, S., Sharma, S., Eleftheriadis, K., Uttal, T., Jefferson, A.J., Bergin, M., Makshtas, A., Tunved, P., & Fiebig, M. (2017). On Aethalometer measurement uncertainties and an instrument correction factor for the Arctic. Atmospheric Measurement Techniques, 10, 5039-5062. DOI:10.5194/AMT-10-5039-2017.

Beegum, S.N., Moorthy, K.K., Babu, S.S., Satheesh, S.K., Vinoj, V., Badarinath, K.V., Safai, P.D., Devara, P.C., Singh, S., Vinod, Dumka, U.C., & Pant, P. (2009). Spatial distribution of aerosol black carbon over India during pre-monsoon season. Atmospheric Environment, 43, 1071-1078. DOI:10.1016/J.ATMOSENV.2008.11.042.

Benchrif, A., Guinot, B., Bounakhla, M., Cachier, H., Damnati, B., & Baghdad, B. (2018). Aerosols in Northern Morocco: Input pathways and their chemical fingerprint. Atmospheric Environment, 174, 140-147. DOI:10.1016/J.ATMOSENV.2017.11.047.

Bernardoni, V., Ferrero, L., Bolzacchini, E., Forello, A.C., Gregorič, A., Massabò, D., Močnik, G., Prati, P., Rigler, M., Santagostini, L., Soldan, F., Valentini, S., Valli, G., & Vecchi, R. (2021). Determination of Aethalometer multiple-scattering enhancement parameters and impact on source apportionment during the winter 2017/18 EMEP/ACTRIS/COLOSSAL campaign in Milan. Atmospheric Measurement Techniques, 14, 2919-2940. DOI:10.5194/AMT-14-2919-2021.

Bibi, S., Alam, K., Chishtie, F.A., Bibi, H., & Rahman, S. (2017). Temporal variation of Black Carbon concentration using Aethalometer observations and its relationships with meteorological variables in Karachi, Pakistan. Journal of Atmospheric and Solar-Terrestrial Physics, 157, 67-77. DOI:10.1016/J.JASTP.2017.03.017.

Botsa, S.M., Magesh, N.S., Tiwari, A.K., & Tara, D. (2021). Characterization of black carbon aerosols over an Indian Antarctic Station, Maitri and identification of potential source areas. Environmental Science: Atmospheres. DOI:10.1039/d1ea00024a.

Carslaw, D. C. and K. Ropkins, (2012) openair - an R package for air quality data analysis. Environmental Modelling & Software. Volume 27-28, 52-61.

Carslaw D. (2021). worldmet: Import Surface Meteorological Data from NOAA Integrated Surface Database (ISD). R package version 0.9.5. https://CRAN.R-project.org/package=worldmet.

Cao, J., Zhu, C., Chow, J.C., Watson, J.G., Han, Y., Wang, G., Shen, Z., & An, Z. (2009). Black carbon relationships with emissions and meteorology in Xi'an, China. Atmospheric Research, 94, 194-202. DOI: 10.1016/J.ATMOSRES.2009.05.009.

Corrigan, C.E., Ramanathan, V., & Schauer, J.J. (2006). Impact of monsoon transitions on the physical and optical properties of aerosols. Journal of Geophysical Research, 111. http://dx.doi.org/10.1029/2005JD006370.

Costabile, F., Alas, H.D., Aufderheide, M., Avino, P., Amato, F., Argentini, S., Barnaba, F., Berico, M., Bernardoni, V., Biondi, R., Calzolai, G., Canepari, S., Casasanta, G., Ciampichetti, S., Conidi, A., Cordelli, E., Ianni, A.D., Liberto, L.D., Facchini, M.C., Facci, A.L., Frascá, D., Gilardoni, S., Grollino, M.G., Gualtieri, M., Lucarelli, F., Malaguti, A., Manigrasso, M., Montagnoli, M., Nava, S., Padoan, E., Perrino, C., Petralia, E., Petenko, I., Querol, X., Simonetti, G., Tranfo, G., Ubertini, S., Valli, G., Valentini, S., Vecchi, R., Volpi, F., Weinhold, K., Wiedensholer, A., Zanini, G., & Gobbi, G.P. (2017). First results of the "Carbonaceous Aerosol in Rome and Environs (CARE)" Experiment: Beyond current standards for PM10. Atmosphere, 8, 249-290. DOI:10.3390/ATMOS8120249.

Costabile, F., Angelini, F., Barnaba, F., & Gobbi, G.P. (2015). Partitioning of Black Carbon between ultrafine and fine particle modes in an urban airport vs. urban background environment. Atmospheric Environment, 102, 136-144. DOI:10.1016/J.ATMOSENV.2014.11.064Corpus ID: 97825083.

Cui, S., Xian, J., Shen, F., Zhang, L., Deng, B., Zhang, Y., & Ge, X. (2021). One-Year Real-Time Measurement of Black Carbon in the Rural Area of Qingdao, Northeastern China: Seasonal Variations, Meteorological Effects, and the COVID-19 Case Analysis. Atmosphere, 12, 394. DOI:10.3390/ATMOS12030394.

Deng, J., Guo, H., Zhang, H., Zhu, J., Wang, X., & Fu, P. (2020). Source apportionment of black carbon aerosols from light absorption observation and source-oriented modeling: an implication in a coastal city in China. Atmospheric Chemistry and Physics. DOI:10.5194/ACP-20-14419-2020.

Duc, H.N., Shingles, K., White, S.J., Salter, D., Chang, L.T., Gunashanhar, G., Riley, M., Trieu, T., Dutt, U., Azzi, M., Beyer, K., Hynes, R.G., & Kirkwood, J. (2020). Spatial-Temporal Pattern of Black Carbon (BC) Emission from Biomass Burning and Anthropogenic Sources in New South Wales and the Greater Metropolitan Region of Sydney, Australia. Atmosphere. DOI:10.3390/atmos11060570.

Deabji, N., Fomba, K.W., El Hajjaji, S., Mellouki, A., & Herrmann, H. (2021). First insights into Northern Africa high-altitude background aerosol chemical composition and source influences. Atmospheric Chemistry and Physics, 1-41. DOI:10.5194/ACP-2021-106.

Djossou, J.H., Léon, J.F., Akpo, A.B., Liousse, C., Yoboué, V., Bedou, M., Bodjrenou, M., Chiron, C., Galy-Lacaux, C., Gardrat, E., Abbey, M., Keita, S., Bahino, J., N'Datchoh, E.T., Ossohou, M., & Awanou, C.N. (2017). Mass concentration, optical depth and carbon composition of particulate matter in the major southern West African cities of Cotonou (Benin) and Abidjan (Côte d'Ivoire). Atmospheric Chemistry and Physics, 18, 6275-6291. DOI:10.5194/ACP-18-6275-2018.

Doumbia, E.H., Liousse, C., Galy-Lacaux, C., Ndiaye, S.A., Diop, B., Ouafo, M., Assamoi, E., Gardrat, E., Castera, P., Rosset, R., Akpo, A.B., & Sigha, L. (2012). Real time black carbon measurements in West and Central Africa urban sites. Atmospheric Environment, 54, 529-537. DOI:10.1016/J.ATMOSENV.2012.02.005.

Draxler, R.R., Rolph, G.D., 2007. HYbrid single-particle lagrangian integrated trajectory model. In: National Air Quality Conference, February 11, 2007. NOAA Air Resource Laboratory. https://www.arl.noaa.gov/documents/workshop/NAQC2007/HTML_Docs/index.html.

Ezani, E., Dhandapani, S., Heal, M.R., Praveena, S.M., Khan, M., & Ramly, Z.T. (2021). Characteristics and Source Apportionment of Black Carbon (BC) in a Suburban Area of Klang Valley, Malaysia. Atmosphere. DOI:10.3390/atmos12060784.

Fossum, K.N., Ovadnevaite, J., Liu, D., Flynn, M., O'Dowd, C.D., & Ceburnis, D. (2022). Background levels of black carbon over remote marine locations. Atmospheric Research. DOI:10.1016/j.atmosres.2022.106119.

Ganguly, D., Jayaraman, A., Gadhavi, H., & Rajesh, T.A. (2005). Features in wavelength dependence of aerosol absorption observed over central India. Geophysical Research Letters, 32. DOI:10.1029/2005GL023023

Gatari, M., & Boman, J. (2003). Black carbon and total carbon measurements at urban and rural sites in Kenya, East Africa. Atmospheric Environment, 37, 1149-1154. DOI:10.1016/S1352-2310(02)01001-4.

Gatari, M., Kinney, P.L., Yan, B., Sclar, E.D., Volavka-Close, N., Ngo, N.S., Mwaniki Gaita, S., Law, A., Ndiba, P.K., Gachanja, A.N., Graeff, J., & Chillrud, S. (2019). High airborne black carbon concentrations measured near roadways in Nairobi, Kenya. Transportation Research Part D: Transport and Environment. DOI :10.1016/J.TRD.2017.10.002.

Genga, A., Ielpo, P., Siciliano, T., & Siciliano, M. (2017). Carbonaceous particles and aerosol mass closure in PM2.5 collected in a port city. Atmospheric Research, 183, 245-254. DOI:10.1016/J.ATMOSRES.2016.08.022.

Gogoi, M.M., Suresh Babu, S., Arun, B., Krishna Moorthy, K., Ajay, A., Ajay, P., Suryavanshi, A.S., Borgohain, A., Guha, A., Shaikh, A., Pathak, B., Gharai, B., Ramasamy, B., Balakrishnaiah, G., Menon, H.B., Kuniyal, J.C., Krishnan, J., Rama Gopal, K., Maheswari, M., Naja, M., Kaur, P., Bhuyan, P.K., Gupta, P., Singh, P., Srivastava, P., Singh, R.S., Kumar, R., Rastogi, S., Kundu, S.S., Kompalli, S.K., Panda, S., Rao, T.C., Das, T., & Kant, Y. (2021). Response of Ambient BC Concentration Across the Indian Region to the Nation-Wide Lockdown: Results from the ARFINET Measurements of ISRO-GBP. Current Science (00113891), 120. DOI:10.18520/cs/v120/i2/341-351.

Giwa, S.O., Adama, O.O., & Akinyemi, O.O. (2014). Baseline black carbon emissions for gas flaring in the Niger Delta region of Nigeria. Journal of Natural Gas Science and Engineering, 20, 373-379. DOI: 10.1016/J.JNGSE.2014.07.026.

Guha, A., De, B.K., Dhar, P., Banik, T., Chakraborty, M., Roy, R., Choudhury, A., Gogoi, M.M., Babu, S.S., & Moorthy, K.K. (2014). Seasonal characteristics of aerosol black carbon in relation to long range transport over Tripura in Northeast India. Aerosol and Air Quality Research, 15, 786-798. DOI:10.4209/AAQR.2014.02.0029.

Grange, S.K., Lewis, A.C., & Carslaw, D.C. (2016). Source apportionment advances using polar plots of bivariate correlation and regression statistics. Atmospheric Environment, 145, 128-134, DOI: 10.1016/J.ATMOSENV.2016.09.016.

Grolemund, G., & Wickham, H. (2011). Dates and Times Made Easy with lubridate. Journal of Statistical Software, 40, 1-25. DOI:10.18637/JSS.V040.I03.

Hansen, A.D.A. (2005) The Aethalometer, Manual. Magee Scientific Company, Berkeley.

Jain, S., Sharma, S.K., Choudhary, N., Masiwal, R., Saxena, M., Sharma, A., Mandal, T.K., Gupta, A., Gupta, N.C., & Sharma, C. (2017). Chemical characteristics and source apportionment of PM2.5 using PCA/APCS, UNMIX, and PMF at an urban site of Delhi, India. Environmental Science and Pollution Research, 24, 14637-14656. DOI:10.1007/s11356-017-8925-5.

Janssen, N.A., Hoek, G., Simic-Lawson, M., Fischer, P., van Bree, L., ten Brink, H., Keuken, M.P., Atkinson, R.W., Anderson, H.R., Brunekreef, B., & Cassee, F.R. (2011). Black Carbon as an Additional Indicator of the Adverse Health Effects of Airborne Particles Compared with PM10 and PM2.5. Environmental Health Perspectives, 119, 1691 - 1699. DOI :10.1289/ehp.1003369.

744 Jonson, J.E., Gauß, M., Schulz, M., Jalkanen, J., & Fagerli, H. (2020). Effects of global ship emissions
745 on European air pollution levels. Atmospheric Chemistry and Physics, 20, 11399-11422.
746 DOI:10.5194/ACP-20-11399-2020.

747 Kalogridis, A., Vratolis, S., Liakakou, E., Gerasopoulos, E., Mihalopoulos, N., & Eleftheriadis, K.
748 (2018). Assessment of wood burning versus fossil fuel contribution to wintertime black carbon and
749 carbon monoxide concentrations in Athens, Greece. Atmos. Chem. Phys., 18, 10219–10236.
750 DOI:10.5194/ACP-18-10219-2018.

751 Khedidji, S., Müller, K., Rabhi, L., Spindler, G., Fomba, K.W., Pinxteren, D.V., Yassaa, N., &
752 Herrmann, H. (2020). Chemical Characterization of Marine Aerosols in a South Mediterranean Coastal
753 Area Located in Bou Ismaïl, Algeria. Aerosol and Air Quality Research, 20, 2448-2473.
754 DOI:10.4209/aaqr.2019.09.0458.

755 Knox, A., Evans, G.J., Brook, J.R., Yao, X., Jeong, C., Godri, K.J., Sabaliauskas, K., & Slowik, J.G.
756 (2009). Mass Absorption Cross-Section of Ambient Black Carbon Aerosol in Relation to Chemical Age.
757 Aerosol Science and Technology, 43, 522 - 532. DOI:10.1080/02786820902777207.

758 Kompalli, S.K., Moorthy, K.K., & Babu, S.S. (2014a). Rapid response of atmospheric BC to
759 anthropogenic sources: observational evidence. Atmospheric Science Letters, 15.
760 DOI:10.1002/asl2.483.

761 Kompalli, S.K., Babu, S.S., Moorthy, K.K., Manoj, M.R., Kumar, N., Shaeb, K.H., & Joshi, A.K.
762 (2014b). Aerosol black carbon characteristics over Central India: Temporal variation and its dependence
763 on mixed layer height. Atmospheric Research, 147, 27-37. DOI:10.1016/J.ATMOSRES.2014.04.015.

764 Lack, D.A., & Corbett, J.J. (2012). Black carbon from ships: a review of the effects of ship speed, fuel
765 quality and exhaust gas scrubbing. Atmospheric Chemistry and Physics, 12, 3985-4000.
766 DOI:10.5194/ACP-12-3985-2012

767 Liu, H., Wang, Q., Xing, L., Zhang, Y., Zhang, T., Ran, W., & Cao, J. (2021). Measurement report:
768 quantifying source contribution of fossil fuels and biomass-burning black carbon aerosol in the
769 southeastern margin of the Tibetan Plateau. Atmospheric Chemistry and Physics. DOI:10.5194/ACP-
770 21-973-2021

771 Mamoudou, I., Aime, K.T., & Njuguna, J.N. (2018). Black Carbon from Ship Emissions: A Review of
772 its Measurement and Estimation Methods, Emissions Factors, Global Emissions, and Impacts.
773 International journal of scientific and research publications, 8. DOI:10.29322/IJSRP.8.3.2018.P7536

774 Martinsson, J., Azeem, H.A., Sporre, M.K., Bergström, R., Ahlberg, E., Öström, E., Kristensson, A.,
775 Swietlicki, E., & Stenström, K. (2016). Carbonaceous aerosol source apportionment using the
776 Aethalometer model – evaluation by radiocarbon and levoglucosan analysis at a rural background site
777 in southern Sweden. Atmospheric Chemistry and Physics, 17, 4265-4281., DOI:10.5194/ACP-17-4265-
778 2017.

779 Mousavi, A., Sowlat, M.H., Hasheminassab, S., Polidori, A., & Sioutas, C. (2018). Spatio-temporal
780 trends and source apportionment of fossil fuel and biomass burning black carbon (BC) in the Los
781 Angeles Basin. The Science of the total environment, 640-641, 1231-1240.
782 DOI:10.1016/j.scitotenv.2018.06.022.

783 NIC special report, (August 2009). North Africa: The Impact of Climate Change to 2030 (Selected
784 Countries). NIC 2009-007D.

785 NOAA, (2020). Accessing data selection screen for Surface Data Hourly Global (DS3505).
786 https://www7.ncdc.noaa.gov/CDO/cdo.

787 Oluleye, A.E., & Folorunsho, A. (2020). Black carbon pollution simulations: a RegCM4 model
788 projection and assessment during the boreal winter and summer over West Africa region. Modeling
789 Earth Systems and Environment, 7, 2313 - 2327. DOI:10.1007/s40808-020-00976-7

790 Pani, S.K., Wang, S., Lin, N., Chantara, S., Lee, C., & Thepnuan, D. (2019). Black carbon over an urban
791 atmosphere in northern peninsular Southeast Asia: Characteristics, source apportionment, and
792 associated health risks. Environmental pollution, 259, 113871. DOI:10.1016/j.envpol.2019.113871

793 Panda, S., Mallik, C., Nath, J., Das, T., & Ramasamy, B. (2020). A study on variation of atmospheric
794 pollutants over Bhubaneswar during imposition of nationwide lockdown in India for the COVID-19
795 pandemic. Air Quality, Atmosphere, & Health. 1 - 12. DOI:10.1007/s11869-020-00916-5.

796 Peng, X., Liu, M., Zhang, Y., Meng, Z.Q., Achal, V., Zhou, T., Long, L., & She, Q. (2019). The
797 characteristics and local-regional contributions of atmospheric black carbon over urban and suburban
798 locations in Shanghai, China. Environmental pollution, 255 Pt 1, 113188.
799 DOI:10.1016/j.envpol.2019.113188

800 Petzold, A., Ogren, J.A., Fiebig, M., Laj, P., Li, S., Baltensperger, U., Holzer-Popp, T., Kinne, S.,
801 Pappalardo, G., Sugimoto, N., Wehrli, C., Wiedensohler, A., & Zhang, X. (2013). Recommendations
802 for the interpretation of "black carbon" measurements. Atmospheric Chemistry and Physics, 13, 9485-
803 9517. DOI:10.5194/ACPD-13-9485-2013.

804 Querol, X., Alastuey, A., Viana, M., Moreno, T., Reche, C., Minguillón, M.C., Ripoll, A., Pandolfi, M.,
805 Amato, F., Karanasiou, A., Pérez, N., Pey, J., Cusack, M., Vázquez, R., Plana, F., Dall'Osto, M., Rosa,
806 J.D., Campa, A.M., Fernández-Camacho, R., Rodríguez, S., Pio, C., Alados-Arboledas, L., Titos, G.,
807 Artíñano, B., Salvador, P., Santos, S.G., & Patier, R.F. (2013). Variability of carbonaceous aerosols in
808 remote, rural, urban and industrial environments in Spain: implications for air quality policy.
809 Atmospheric Chemistry and Physics, 13, 6185-6206. DOI:10.5194/ACP-13-6185-2013.

810 R Core Team (2020). R: A language and environment for statistical computing. R Foundation for
811 Statistical Computing, Vienna, Austria. URL https://www.R-project.org/.

812 Ramachandran, S., and T. A. Rajesh. (2007), Black carbon aerosol mass concentrations over
813 Ahmedabad, an urban location in western India: Comparison with urban sites in Asia, Europe, Canada,
814 and the United States, J. Geophys. Res., 112, D06211, DOI:10.1029/2006JD007488.

815 Ran, L., Deng, Z., Wang, P.C., & Xia, X. (2016). Black carbon and wavelength-dependent aerosol
816 absorption in the North China Plain based on two-year aethalometer measurements. Atmospheric
817 Environment, 142, 132-144. DOI:10.1016/J.ATMOSENV.2016.07.014

818 Rolph, G., Stein, A.F., & Stunder, B. (2017). Real-time Environmental Applications and Display
819 sYstem: READY. Environ. Model. Softw., 95, 210-228. DOI:10.1016/j.envsoft.2017.06.025.

820 Rivellini, L., Chiapello, I., Tison, E., Fourmentin, M., Féron, A., Diallo, A., Ndiaye, T., Goloub, P.,
821 Canonaco, F., Prévôt, A.S., & Riffault, V. (2017). Chemical characterization and source apportionment
822 of submicron aerosols measured in Senegal during the 2015 SHADOW campaign. Atmospheric
823 Chemistry and Physics, 17, 10291-10314. DOI:10.5194/ACP-17-10291-2017

824 Reche, C., Querol, X., Alastuey, A., Viana, M., Pey, J., Moreno, T., Rodríguez, S., González, Y.,
825 Fernández-Camacho, R., Rosa, J.D., Dall'Osto, M., Prévôt, A.S., Hueglin, C., Harrison, R.M., &

826 Quincey, P.G. (2011). New considerations for PM, Black Carbon and particle number concentration for
827 air quality monitoring across different European cities. Atmospheric Chemistry and Physics, 11, 6207-
828 6227. DOI:10.5194/acp-11-6207-2011.

829 Reche, C., Viana, M., Amato, F., Alastuey, A., Moreno, T., Hillamo, R., Teinilä, K., Saarnio, K., Seco,
830 R., Peñuelas, J., Mohr, C., Prévôt, A.S., & Querol, X. (2012). Biomass burning contributions to urban
831 aerosols in a coastal Mediterranean city. The Science of the total environment, 427-428, 175-90. DOI:
832 10.1016/j.scitotenv.2012.04.012.

833 Safai, P., Kewat, S., Praveen, P., Rao, P., Momin, G., Ali, K., Devara, P., (2007). Seasonal variation of
834 black carbon aerosols over a tropical urban city of Pune, India. Atmos. Environ. 41, 2699–2709. DOI:
835 10.1016/j.atmosenv.2006.11.044.

836 Schmid, O., Artaxo, P., Arnott, W.P., Chand, D., Gatti, L.V., Frank, G.P., Hoffer, A., Schnaiter, M., &
837 Andreae, M.O. (2005). Spectral light absorption by ambient aerosols influenced by biomass burning in
838 the Amazon Basin. I: Comparison and field calibration of absorption measurement techniques.
839 Atmospheric Chemistry and Physics, 6, 3443-3462. DOI:10.5194/ACP-6-3443-2006.

840 Segersson, D., Eneroth, K., Gidhagen, L., Johansson, C., Omstedt, G., Engström Nylén, A., & Forsberg,
841 B. (2017). Health Impact of PM10, PM2.5 and Black Carbon Exposure Due to Different Source Sectors
842 in Stockholm, Gothenburg and Umea, Sweden. International Journal of Environmental Research and
843 Public Health, 14. DOI:10.3390/ijerph14070742.

844 Stein, A.F., Draxler, R.R., Rolph, G., Stunder, B., Cohen, M.D., & Ngan, F. (2015). NOAA's HYSPLIT
845 Atmospheric Transport and Dispersion Modeling System. Bulletin of the American Meteorological
846 Society, 96, 2059-2077. DOI:10.1175/BAMS-D-14-00110.1.

847 Srivastava, S., Kumar, M., Singh, R.S., Rai, B.N., Mall, R.K., & Banerjee, T. (2019). Long-term
848 observation of black carbon aerosols at an urban location over the central Indo-Gangetic Plain, South
849 Asia. Atmósfera. DOI:10.20937/ATM.2019.32.02.02.

850 Sun, J.Y., Wu, C., Wu, D., Cheng, C., Li, M., Li, L., Deng, T., Yu, J.Z., Li, Y.J., Zhou, Q., Liang, Y.,
851 Sun, T., Song, L., Cheng, P., Yang, W., Pei, C., Chen, Y., Cen, Y., Nian, H., & Zhou, Z. (2020a).
852 Amplification of black carbon light absorption induced by atmospheric aging: temporal variation at
853 seasonal and diel scales in urban Guangzhou. Atmospheric Chemistry and Physics, 20, 2445-2470.
854 DOI:10.5194/acp-20-2445-2020.

855 Sun, T., Wu, C., Wu, D., Liu, B., Sun, J.Y., Mao, X., Yang, H., Deng, T., Song, L., Li, M., Li, Y.J., &
856 Zhou, Z. (2020b). Time-resolved black carbon aerosol vertical distribution measurements using a 356-
857 m meteorological tower in Shenzhen. Theoretical and Applied Climatology, 140, 1263-1276.
858 DOI:10.1007/s00704-020-03168-6.

859 Tefera, W., Kumie, A., Berhane, K., Gilliland, F.D., Lai, A.M., Sricharoenvech, P., Samet, J.M., Patz,
860 J.A., & Schauer, J.J. (2020). Chemical Characterization and Seasonality of Ambient Particles (PM2.5)
861 in the City Centre of Addis Ababa. International Journal of Environmental Research and Public
862 Health, 17. DOI:10.3390/ijerph17196998.

863 Tiwari, S., Srivastava, A., Bisht, D.S., Parmita, P., Srivastava, M.K., & Attri, S.D. (2013). Diurnal and
864 seasonal variations of black carbon and PM2.5 over New Delhi, India: Influence of meteorology.
865 Atmospheric Research, 125, 50-62. DOI:10.1016/J.ATMOSRES.2013.01.011

866 Wang, Q., Liu, H., Ye, J., Tian, J., Zhang, T., Zhang, Y., Liu, S., & Cao, J. (2020). Estimating Absorption
867 Ångström Exponent of Black Carbon Aerosol by Coupling Multiwavelength Absorption with Chemical
868 Composition. Environmental Science and Technology Letters. DOI:10.1021/acs.estlett.0c00829

Wang, Q., Cao, J., Han, Y., Tian, J., Zhu, C., Zhang, Y., Zhang, N., Shen, Z., Ni, H., Zhao, S., & Wu, J. (2018). Sources and physicochemical characteristics of black carbon aerosol from the southeastern Tibetan Plateau: internal mixing enhances light absorption. Atmospheric Chemistry and Physics, 18, 4639-4656., DOI:10.5194/ACP-18-4639-2018.

Wang, Y.Q., Zhang, X.Y. and Draxler, R. (2009). TrajStat: GIS-based software that uses various trajectory statistical analysis methods to identify potential sources from long-term air pollution measurement data. Environmental Modelling & Software, 24: 938-939. 10.1016/j.envsoft.2009.01.004.

WHO global air quality guidelines. Particulate matter (PM2.5 and PM10), ozone, nitrogen dioxide, sulfur dioxide and carbon monoxide. Geneva: World Health Organization; 2021. Licence: CC BY-NC-SA 3.0 IGO.

Wickham H. (2016). ggplot2: Elegant Graphics for Data Analysis. Springer-Verlag New York. ISBN 978-3-319-24277-4, http://ggplot2.org.

Wickham H., François R., Henry L. and Müller K. (2021). dplyr: A Grammar of Data Manipulation. R package version 1.0.5. https://CRAN.R-project.org/package=dplyr.

Xu, L., Zhang, J., Sun, X., Xu, S., Shan, M., Yuan, Q., Liu, L., Du, Z., Liu, D., Xu, D., Song, C., Liu, B., Lu, G., Shi, Z., & Li, W. (2020). Variation in Concentration and Sources of Black Carbon in a Megacity of China During the COVID-19 Pandemic. Geophysical Research Letters, 47. DOI:10.1029/2020GL090444.

Xulu, N.A., Piketh, S.J., Feig, G., Lack, D.A., & Garland, R.M. (2020). Characterizing Light-absorbing Aerosols in a Low-income Settlement in South Africa. Aerosol and Air Quality Research, 20, 1812-1832. DOI:10.4209/aaqr.2019.09.0443.

Zanatta, M., Gysel, M., Bukowiecki, N., Müller, T.J., Weingartner, E., Areskoug, H., Fiebig, M., Yttri, K.E., Mihalopoulos, N., Kouvarakis, G., Beddows, D.C., Harrison, R.M., Cavalli, F., Putaud, J., Spindler, G., Wiedensohler, A., Alastuey, A., Pandolfi, M., Sellegri, K., Swietlicki, E., Jaffrezo, J.L., Baltensperger, U., & Laj, P. (2016). A European aerosol phenomenology-5 : Climatology of black carbon optical properties at 9 regional background sites across Europe. Atmospheric Environment, 145, 346-364. DOI:10.1016/J.ATMOSENV.2016.09.035.

Zotter, P., Herich, H., Gysel, M., El-Haddad, I., Zhang, Y., Močnik, G., Hüglin, C., Baltensperger, U., Szidat, S., & Prévôt, A.S. (2016). Evaluation of the absorption Ångström exponents for traffic and wood burning in the Aethalometer-based source apportionment using radiocarbon measurements of ambient aerosol. Atmospheric Chemistry and Physics, 17, 4229-4249. DOI:10.5194/ACP-17-4229-2017.

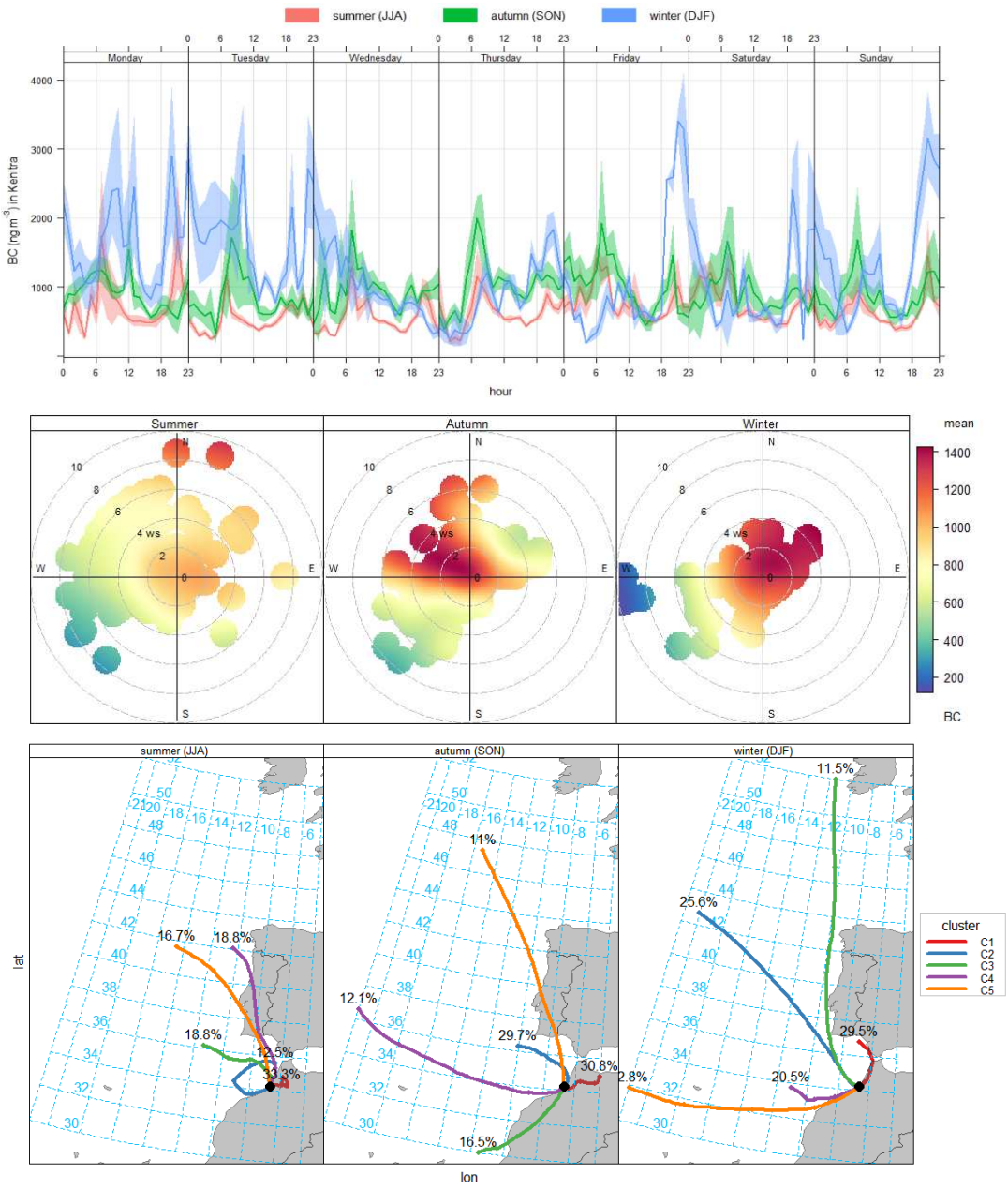
summer (JJA)
autumn (SON)
winter (DJF)
Monday
Tuesday
Wednesday
Thursday
Friday
Saturday
Sunday
BC (ng.m-3) in Kenitra
hour
Summer
Autumn
Winter
mean
BC
4 ws
summer (JJA)
autumn (SON)
winter (DJF)
lat
lon
cluster
C1
C2
C3
C4
C5
16.7%
18.8%
18.8%
12.5%
11.3%
11%
12.1%
29.7%
30.8%
16.5%
11.5%
25.6%
29.5%
20.5%
2.8%